國立臺灣大學電機資訊學院光電工程學研究所

碩士論文

Graduate Institute of Photonics and Optoelectronics

College of Electrical Engineering and Computer Science

National Taiwan University

Master's Thesis

量子點光阻對於新穎砷化鎵太陽能電池之影響及應用

The application and effects of quantum dots photoresist on the novel GaAs-based solar cells

鄧韜

Tao Deng

指導教授：林建中 教授

Advisor: Professor Chien-Chung Lin

中華民國一一三年十二月

December 2024

doi:10.6342/NTU202500081

摘要

在我的研究中做出了 1mm,2mm3mm 三種尺寸以及 square,hollow square, cross 及 u-shape 四種形狀的砷化鎵(GaAs)太陽能電池，分別用了兩種 anti-reflection coating(ALD+PECVD/PECVD)並研究其在側面加上量子點光阻(QDPR)後的各種特性改變，包含了短路電流、開路電壓、暗電流、量子效率、填充因子、理想因子跟串聯電阻等。期望可以利用 Luminescent down-shifting 效應來幫助元件達成更高的效率。

其中在回字形 2000um 的元件我們觀察到最佳的表現，短路電流密度從 13.6mA/cm^2上升到 19.8 mA/cm^2。相當於 45%的提升，其他形狀的元件也有一定的提升，我們從中看到了很大的潛力，未來會朝著優化製程找到最佳參數以及嘗試更多層量子點光阻繼續努力，我們也嘗試了 triple junctionSolar cell 的製程，目前尚未找到正確的製程方法。我們討論了試過的方法，並持續搜尋可能的解答。

doi:10.6342/NTU202500081

Abstract

In this study, we fabricated GaAs solar cells of three different sizes and four different shapes, applying two types of anti-reflection coatings (ALD+PECVD/PECVD). We investigated the changes in various characteristics after adding quantum dot photoresist (QDPR) to the sidewalls, including short-circuit current, open-circuit voltage, dark current, quantum efficiency, fill factor, ideality factor, and series resistance. The goal is to enhance device efficiency using the luminescent down-shifting (LDS) effect.

Among the devices, the 2000 μm ring-shaped cell demonstrated the best performance, with the short-circuit current density increasing from 13.6 mA/cm² to 19.8 mA/cm², representing a 45% improvement. Other device shapes also showed significant improvements, indicating great potential. In the future, we aim to optimize the fabrication process to determine the best parameters and explore the use of multiple layers of quantum dot photoresist.

We also attempted to fabricate triple-junction solar cells but have not yet identified the correct process. Finally, we discussed the methods we tried and continue to explore possible solutions.

doi:10.6342/NTU202500081

致謝

兩年多來的研究所生活獲得了許多的幫助，從進來時教我們做實驗的舜杰、老密、張境到長庚大學電子系蔡佳龍教授出借量測儀器，以及蔡教授的碩士生徐承凱幫忙量測，也要感謝工研院電光所梁凱玲工程師及林素芳工程師提供了許多製程上以及專業知識的指導，還要感謝同屆的同學仲辰、皓任、子嘉、挺之、科熹以及學弟妹一路上的幫助與陪伴讓研究生活多了許多樂趣，接下來要感謝指導教授林建中教授，從碩一進來實驗室開始就感覺到老師對我們的關心，除了研究上為我們解答更在生活上時時關心我們，從研究方法擴大到面對未來生活的態度都為我們做了很好的示範，很慶幸是在教授的實驗室完成碩士學業。

最後感謝家人朋友的支持讓我有動力完成碩士學業。

doi:10.6342/NTU202500081

Content

doi:10.6342/NTU202500081

doi:10.6342/NTU202500081

List of figure

doi:10.6342/NTU202500081

doi:10.6342/NTU202500081

List of table

doi:10.6342/NTU202500081

CHAPTER 1 Introduction

1.1 History of Solar Cells

The photovoltaic effect was first discovered in 1839 by French physicist Alexandre-Edmond Becquerel[1]. As understanding of semiconductor properties advanced, along with improvements in processing technology, researchers at Bell Labs in the United States found in 1954 that introducing a certain amount of impurities into silicon increased its sensitivity to light[2]. This discovery led to the creation of the first solar cell with practical applications.

Photovoltaic technology is rapidly becoming an important renewable alternative to traditional fossil fuel power generation. By the 1960s, solar cells were already being used as energy sources for artificial satellites[3]. The oil crisis in the 1970s underscored the need for alternative energy sources, further promoting the development of photovoltaic technology for terrestrial use. Today, there are many types of materials used in solar cells, including amorphous silicon[4], polycrystalline silicon[5], CdTe, CuInxGa(1-x)Se2, as well as materials formed by bonding elements from Groups III-V or II-VI of the periodic table.

1.2 Gallium arsenide solar cell

Gallium arsenide (GaAs) [6]is a III-V compound semiconductor material that appears as a bright gray substance with a metallic luster. It has shown excellent performance as an emerging substrate material for solar cells. Compared to silicon-based solar cells with a

doi:10.6342/NTU202500081

theoretical conversion efficiency of 23%, single-junction GaAs solar cells can achieve a theoretical conversion efficiency of up to 27%, while multi-junction GaAs cells can reach as high as 50%[7]. It is considered a promising solar cell technology for the future.

1.3 Quantum Dots photoresist

The QDPR used in this experiment was provided by ITRI and synthesized using CdSe/ZnS core/shell quantum dots, TiO2, dispersant, and negative photoresist, with the red quantum dots at a weight concentration of 10−30 wt%.[8]

1.4 Luminescent Down-Shifting(LDS)

Luminescent Down-Shifting (LDS) is primarily applied in solar cells to enhance their efficiency. The basic principle involves using a thin film or coating containing luminescent materials to convert shorter-wavelength (high-energy) ultraviolet or blue light into longer-wavelength (lower-energy) visible light, thereby reducing UV damage to the solar cell and improving energy absorption. High-energy photons can be absorbed over short distances, but the generated electron-hole pairs are near the semiconductor surface, where recombination losses are significant. In our work, we selected quantum dot photoresist(QDPR) as the LDS material.[9-11]

1.5 Motivation

As the global population continues to grow and electricity demand rises, traditional power

doi:10.6342/NTU202500081

generation methods face increasing environmental pollution challenges. Solar power has emerged as a cleaner energy solution. We aim to maximize solar energy conversion efficiency through innovative device design by incorporating the LDS effect of quantum dots.

doi:10.6342/NTU202500081

Chaptor 2 Working principle and index of Solar cell

2.1 Solar Radiation

The energy emitted by the Sun originates from nuclear fusion reactions, in which hydrogen transforms into helium. The mass loss during this process is converted into electromagnetic radiation through Einstein's relation,E = mc^2. The Sun's current total mass is approximately 2×10302 \times 10^2×1030 kg, and its life cycle is estimated to exceed 10 billion years.

The solar radiation intensity at the average distance of Earth's orbit around the Sun is defined as the solar constant, approximately 1367 W/m², known as AM0. Air mass (AM) is defined as 1/cos(θ), where θ is the angle between the vertical line and the position of the Sun. On Earth, solar irradiance is specified by the AM1.5 spectrum, representing a 48-degree angle from the vertical line. At this angle, the incident solar power is about 963 W/m².

2.2 Working principle

When the energy of an incoming photon exceeds the bandgap of the material, electron-hole pairs are created within the device. In p-type materials, electrons, and in n-type materials, holes only exist temporarily, as they recombine after a period determined by their minority carrier lifetime. Once recombination occurs, the light-generated electron-hole pairs are lost, and the cell can no longer produce current or power. To prevent this loss, the p-n junction collects

doi:10.6342/NTU202500081

the carriers. If a light-generated minority carrier reaches the junction, it is swept across by the electric field, becoming a majority carrier on the other side. In the case of a short-circuited solar cell, these carriers flow through the external circuit, generating current.[12-14]

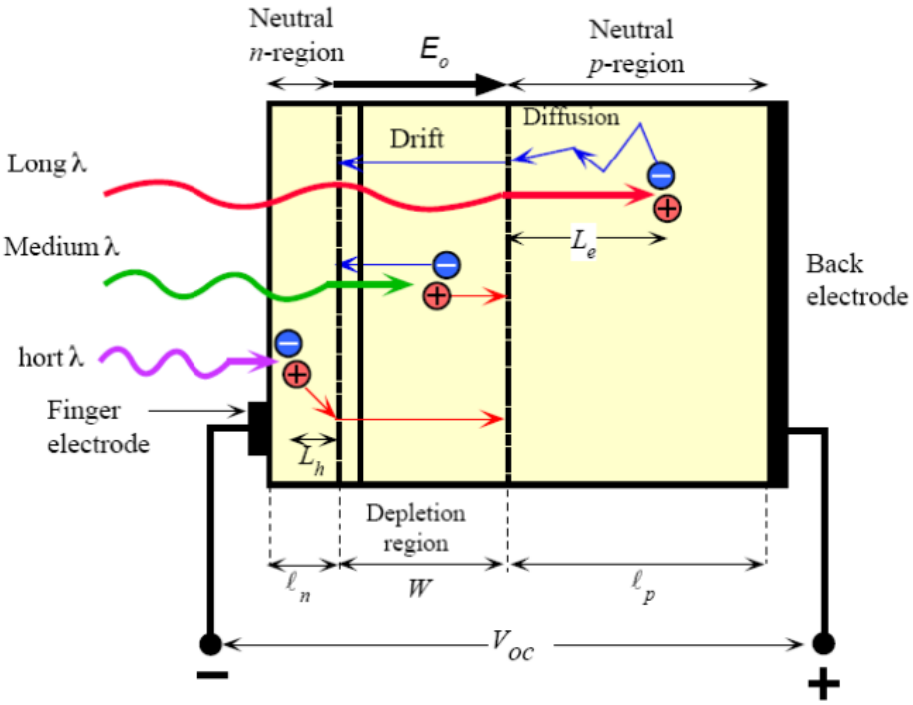

Figure 2.1 Illustrations of solar cell working principle.[13]

2.2.1 Parameters of Solar Cells

When conducting measurements on a solar cell, we obtain a voltage difference, and this voltage difference generates a current. The current can be written as：

$$\mathrm{I}=I_L - I_0(e^{\frac{qv}{nkT}} - 1)$$

2.2.2 Short-Circuit Current

The short-circuit current (Isc) in a solar cell refers to the current generated when the cell's output terminals are directly connected, enabling the maximum possible current to flow.

doi:10.6342/NTU202500081

It is primarily determined by the amount of sunlight absorbed by the cell, the efficiency of converting photons into electrons, and the quality of the cell material.

$$I_{SC} = I_L$$

2.2.3 Open Circuit Voltage

The open-circuit voltage (Voc) of a solar cell is the maximum voltage can produced by device when it is not connected to an external load or circuit . The open-circuit voltage (Voc) is influenced by factors such as the material properties, the junction quality, and the cell's temperature. It signifies the maximum voltage that can be produced by the solar cell and is a crucial factor in assessing the efficiency of energy conversion.

$$V_{oc} = \frac{kT}{q} \ln \left(\frac{I_{sc}}{I_0} + 1\right)$$

2.2.4 Fill Factor

The fill factor indicates "squareness" of the current-voltage (I-V) curve of the solar cell; a higher fill factor means a more efficient cell. Factors that can affect the FF include the series and shunt resistances within the cell, with ideal cells typically achieving a fill factor above 0.75. FF is essential for assessing the overall power conversion efficiency of a solar cell.[15]

$$FF = \frac{P_{max}}{V_{oc}\, I_{sc}}$$

2.2.5 Conversion Efficiency

Conversion Efficiency (η) of a solar cell is the ratio of the electrical power output (Pout)

doi:10.6342/NTU202500081

to the solar power input (Pin) received by the cell. It is typically expressed as a percentage and represents the cell's ability to convert incident sunlight into usable electricity.

$$\eta = \frac{P_m}{P_s} = \frac{J_{sc}\, V_{oc}\, I_{sc}}{P_s}$$

2.2.6 External Quantum Efficiency

External Quantum Efficiency (EQE) is the measure of how effectively a solar cell converts photons of a specific wavelength into electrons. EQE is wavelength-dependent and is typically expressed as a percentage. It shows the number of charge carriers generated and collected for each incident photon, indicating the effectiveness of the cell's light absorption and charge collection.

$$EQE = \frac{electrons/_{sec}}{photons/_{sec}} \times 100\%$$

2.2.7 Ideality Factor

Ideality Factor (n) indicates how closely a solar cell follows ideal diode behavior, typically ranging from 1 to 2. A value near 1 suggests minimal recombination losses, while values closer to 2 indicate significant recombination. This factor helps assess the quality and efficiency of the cell's design. [16]

$$I = I_0(exp(\frac{qV}{nkT}) - 1)$$

doi:10.6342/NTU202500081

2.2.8 Series Resistance

Series Resistance (Rs) in a solar cell is the internal resistance to current flow caused by the cell's components, such as contacts and the semiconductor material. Higher Rs reduces the cell's current output and efficiency, especially in high-light conditions, and is ideally minimized to improve performance.[17]

$$R_s = -\frac{dV}{dI}$$

2.3 Paper review

2.3.1 Enhancement of power conversion efficiency in GaAs solar cells with dual-layer quantum dots using flexible PDMS film.

Figure 2.2 illustrates the schematic of a dual-layer QDs-PDMS film solar cell, utilizing

doi:10.6342/NTU202500081

460 nm quantum dots and PDMS as a material to separate the two layers while also confining the quantum dots.

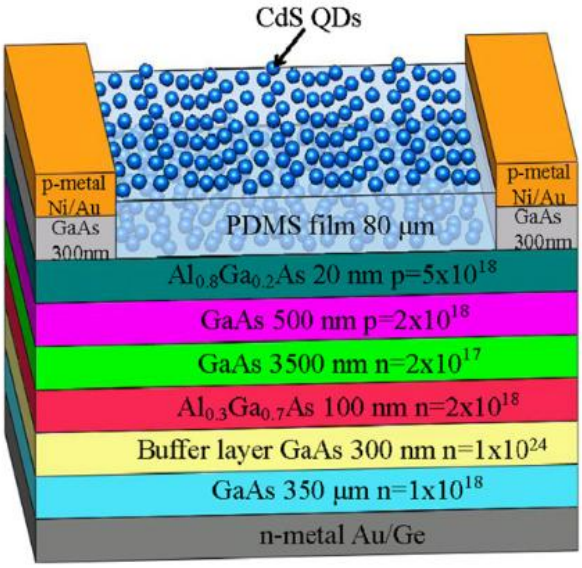

Figure 2.2 schematic of a dual-layer QDs-PDMS film solar cell[10]

Figure 2.3 shows the comparison of the IV curves between devices with dual-layer QDs and those without QDs. The Jsc increased from 19.87mA/cm^2 to 23.52 mA/cm^2, and the PCE improved from 14.36% to 17.45%, corresponding to a 22% enhancement.

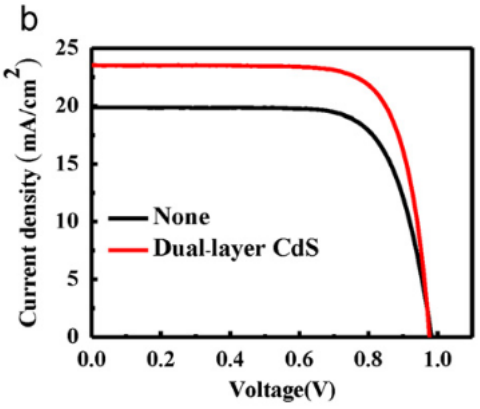

Figure 2.3 JV-curve comparison of devices with and without QDs[10]

Figure 2.4 shows the reflectance comparison of the two devices.With the addition of dual-layer QDs, the surface reflectance also changed. The reduced reflectance indicates higher

doi:10.6342/NTU202500081

light extraction efficiency, which is one of the reasons for the improved PCE.

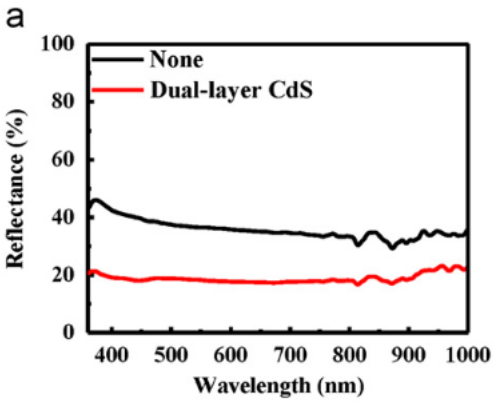

Figure 2.4 Reflectance comparison of devices with and without QDs[10]

2.3.2 Resistance to edge recombination in GaAs-based dots-in-a well Solar cells

This study compares the behavior of light and dark currents in DWELL-structured solar cells and conventional solar cells. The DWELL structure maintains a high Jsc even in smaller devices. In contrast, the Jsc of the control group decreases as the device size decreases due to edge recombination. From the perspective of dark current, smaller devices in the control group exhibit higher dark current, which originates from edge recombination. However, the dark current results of the DWELL structure indicate that it effectively addresses the issue of edge

doi:10.6342/NTU202500081

recombination.

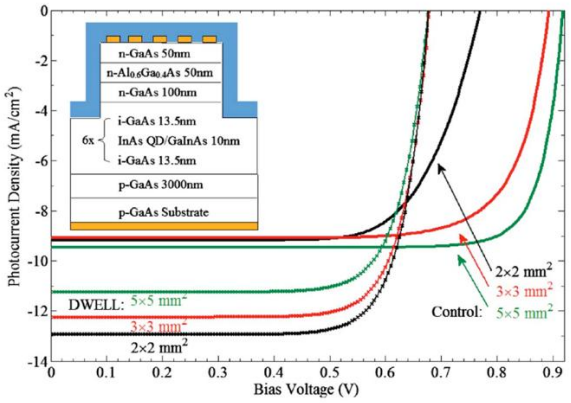

Figure 2.5 Photocurrent of samples[18]

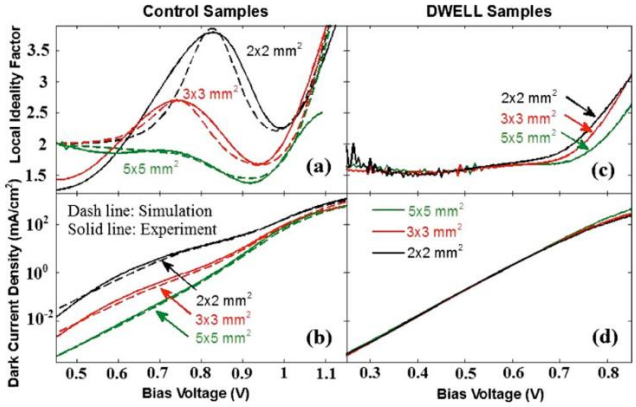

Figure 2.6 Dark current and ideality factor of samples[18]

2.3.3 The luminescent down shifting effect of single-junction GaAs Solar cell with perovskite Quantum Dots

Short-wavelength photons (e.g., UV) are efficiently absorbed within a short distance in solar cells, but this often leads to surface recombination, resulting in photon loss. One solution to this issue is converting short-wavelength light into longer wavelengths, a process known as luminescent down-shifting (LDS). Quantum dots (QDs) are excellent LDS materials. This study uses 514 nm perovskite quantum dots mixed with PDMS as the LDS material and compares the performance of devices with and without QDs. It also examines the differences in

doi:10.6342/NTU202500081

JscJ_{\text{sc}}Jsc, EQE, PCE, and reflectance between QDs with and without baking, showing performance enhancement in both cases after the addition of QDs.

Additionally, this study discusses using PDMS as an encapsulation material for storage lifetime tests, achieving significant improvements over traditional direct-drop QD methods. After 150 hours, the QDs showed no significant performance degradation.

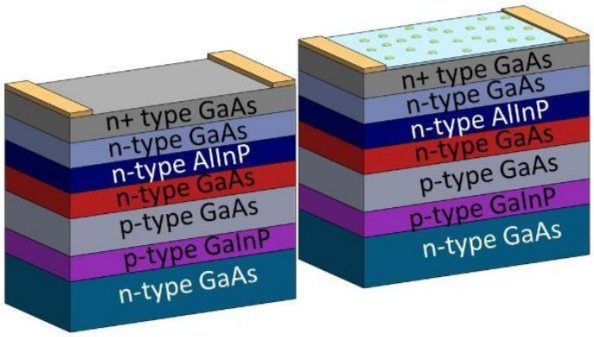

Figure 2.7 Schematic diagram of devices[19]

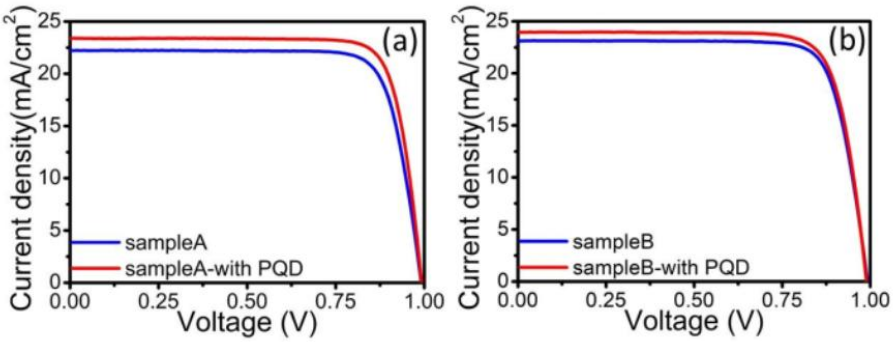

Figure 2.8 JV-curve of two samples[19]

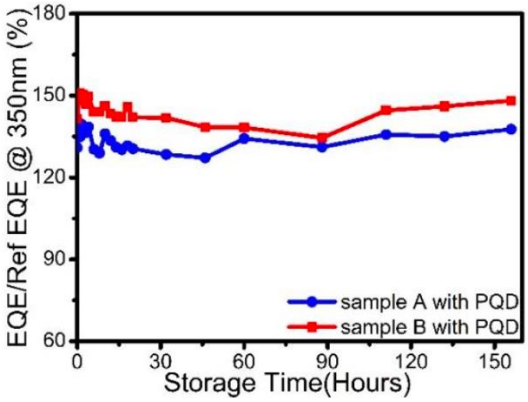

Figure 2.9 The storage lifetime teest of two samples[19]

doi:10.6342/NTU202500081

Chaptor 3 Experiment process and Measurement set up

3.1 Process flow of GaAs Solar cell

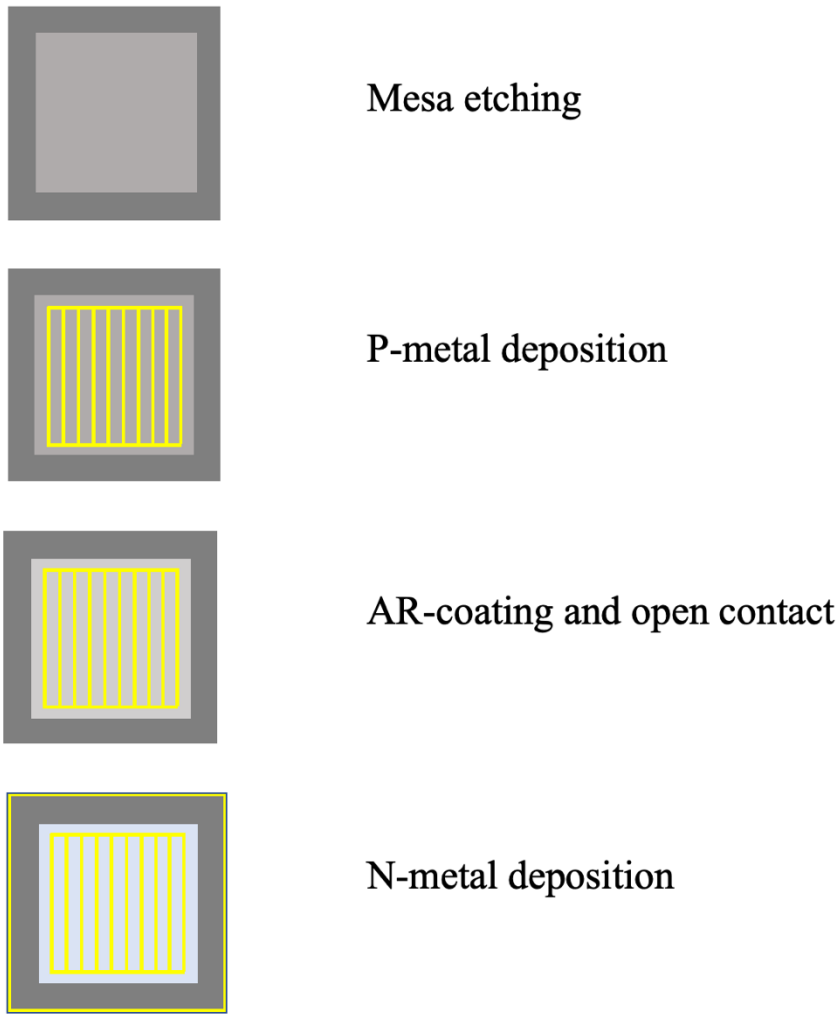

Figure 3.1 Process flow of GaAs solar cell

The wafer used in our experiment was a 4-inch wafer, which we cut into 3.5 x 3.5 cm pieces using a diamond scribe. Before each step, we first cleaned the pieces using acetone in an ultrasonic cleaner, followed by isopropanol and DI water. In the first step, we used S1813 photoresist as a mask and performed ICP(Inductively coupled plasma) dry etching to define

doi:10.6342/NTU202500081

the pattern. The etching depth was around 1400 nm, considering the thickness of the p-doped epitaxial layer and the requirements for subsequent Quantum dots photoresist combination.

The second step was p-metal deposition. We used HMDS and AZ5214 photoresist, which was reversed-baked to form a negative resist. After exposure and development, the p-metal pattern was defined. The developer used was MF319. After development, we performed metal deposition using an e-beam evaporator, with Ti/Pt/Au (200/50/2000 Å) as the metals. Once deposition was completed, we used acetone for lift-off to remove the unwanted metal.

The third step was window etching, a process specific to solar cells that can enhance their conversion efficiency. For this step, we used wet etching. S1813 photoresist was used as a mask to protect the p-metal, and then a solution of phosphoric acid, hydrogen peroxide, and water in a ratio of 1:2:40 was used to remove the GaAs window layer at the top of the epitaxial wafer.

The fourth step was AR-coating. We prepared two versions: one with SiO2 (88 nm) and another with Al2O3 and SiO2 (40/48 nm). After depositing the AR-coating, we needed to open the contact areas to expose them for needle measurements. First, we used HMDS as an adhesive to reduce lateral etching in BOE, then AZ5214 photoresist, reversed to a negative resist, was used as a mask. For the exposed contact areas, we used BOE wet etching to remove the SiO2 or Al2O3 covering the contacts.

The fifth step was N-metal deposition on the back, using GeAu/Au with thicknesses of 200/2000 nm. The GeAu was deposited using a thermal evaporator, while Au was deposited

doi:10.6342/NTU202500081

using an e-beam evaporator. The GeAu forms an ohmic contact with the GaAs substrate, while the Au serves as a conductive layer to enhance conductivity. With this, the basic device was completed. Subsequently, we added Quantum dots photoresist on the sides of the device in an attempt to improve its performance. Measurement results will be discussed in the following sections.[20-23]

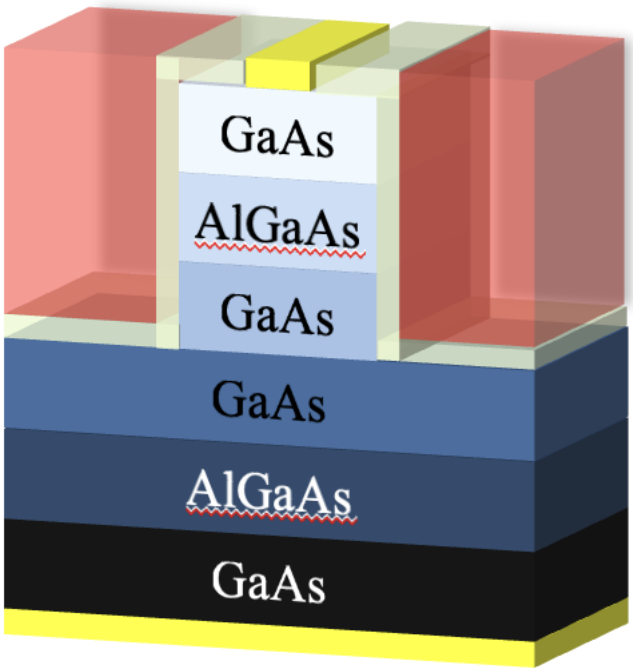

Figure 3.2 Diagram of processed device

3.2 GaAs solar cell with QDPR

Applying quantum dots photoresist (QDPR) to solar cells can theoretically improve the efficiency of solar cells by enhancing light absorption range, increasing carrier generation, reducing energy loss, and improving antireflection properties. Therefore, QDPR is a potential technology for effectively enhancing the performance of solar cells.

doi:10.6342/NTU202500081

3.3 Experimental instrument

3.3.1 Spin coater

We use the YOTEC ASC-80 model spin coater for applying S1813, HMDS, and AZ5214.

Figure 3.3 Spin coater

3.3.2 Hot plate

We use the YOTEC GX-66SB model hot plate to heat the devices after photoresist coating.

doi:10.6342/NTU202500081

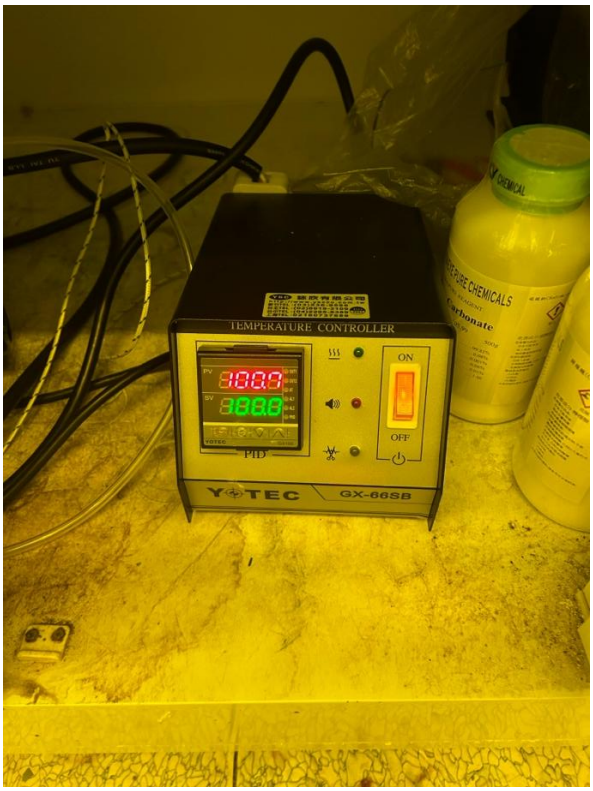

Figure 3.4Hot plate

Figure 3.5 Hot plate

doi:10.6342/NTU202500081

3.3.3 Ultrasonic cleaner

Figure 3.6 Ultrasonic cleaner

3.3.4 Surface profiler

We use the Bruker Dektak XT surface profiler for depth and thickness measurements.

Figure 3.7 Surface profiler

doi:10.6342/NTU202500081

3.3.5 Inductively Coupled Plasma(ICP)

The method of using plasma-enhanced reactive ion gas bombardment to etch target materials is a common etching technique in the semiconductor industry. It is characterized by a fast etching rate, high selectivity, and anisotropy, providing excellent profile control. In our experiment, we used ULVAC's CE-300I for etching the mesa pattern.

Figure 3.8 Inductively coupled plasma

doi:10.6342/NTU202500081

3.3.6 Plasma Enhanced Chemical Vapor Deposition(PECVD)

PECVD (Plasma-Enhanced Chemical Vapor Deposition) is a method used to deposit thin films at lower temperatures by enhancing chemical reactions with plasma. It's commonly used in semiconductor and electronics industries for materials like silicon dioxide and silicon nitride. PECVD offers good film quality, uniformity, and is suitable for temperature-sensitive substrates, making it useful for applications like semiconductor devices and solar cells. In our experiment, we used PECVD to deposit SiO_2.

Figure 3.9 Plasma enhanced chemical vapor deposition

doi:10.6342/NTU202500081

3.3.7 Atomic layer Deposition(ALD)

Atomic Layer Deposition (ALD) is a technique that deposits materials layer by layer in the form of a single atomic layer on a substrate. By controlling the number of deposition cycles, it allows precise control over the film thickness. ALD is used for nanoscale or atomic-scale thin film deposition. In our experiment, we used it to deposit Al_2O_3.

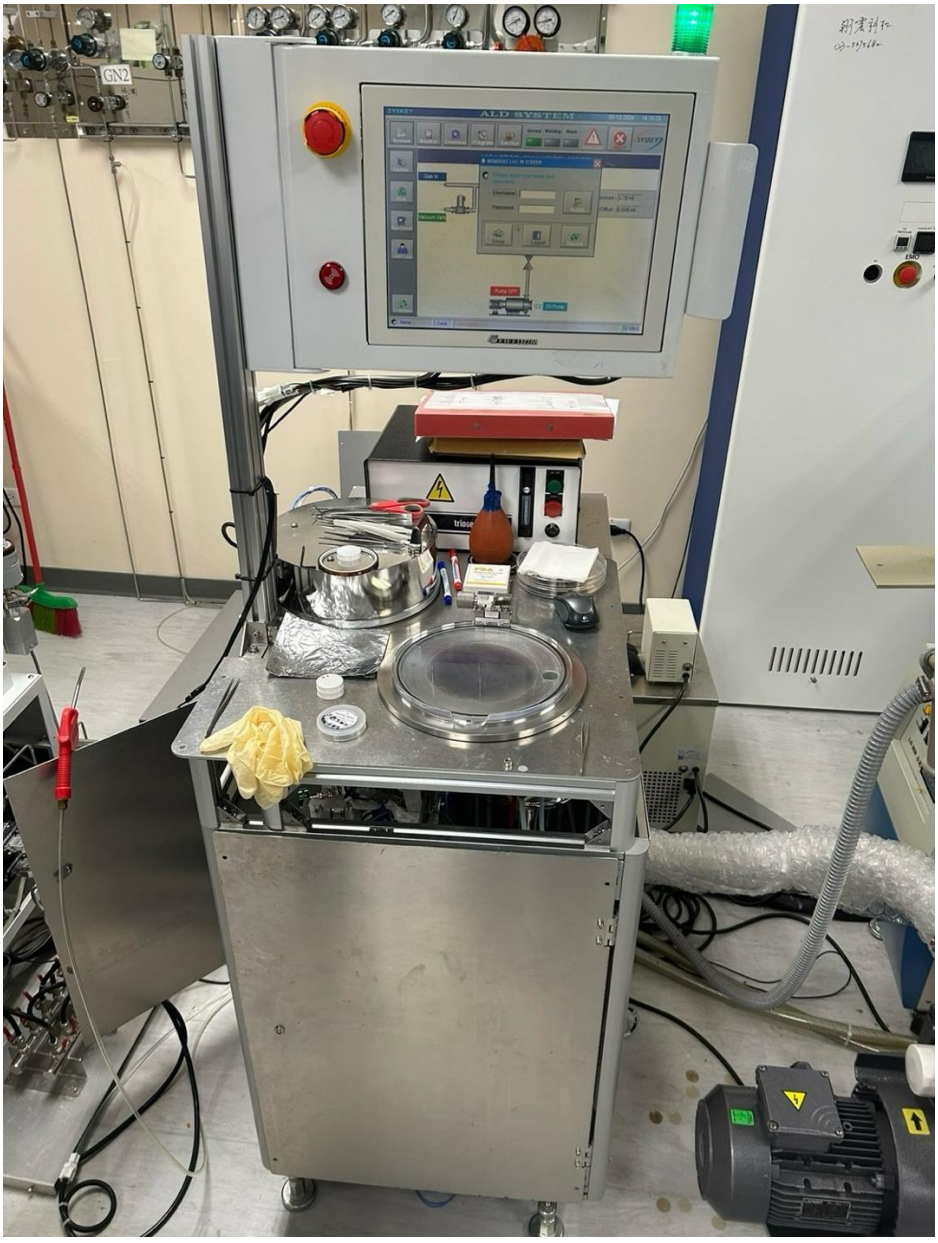

Figure 3.10 Atomic layer deposition

doi:10.6342/NTU202500081

3.3.8 Mask Aligner

In semiconductor fabrication, nearly every step necessitates the use of a photolithography tool. For our exposure process, we employ the SUSS MicroTec MA6 aligner, utilizing a 275-watt mercury lamp with a wavelength of 400 nm as the light source. After positioning the 5-inch mask, manual alignment is executed through an optical microscope.

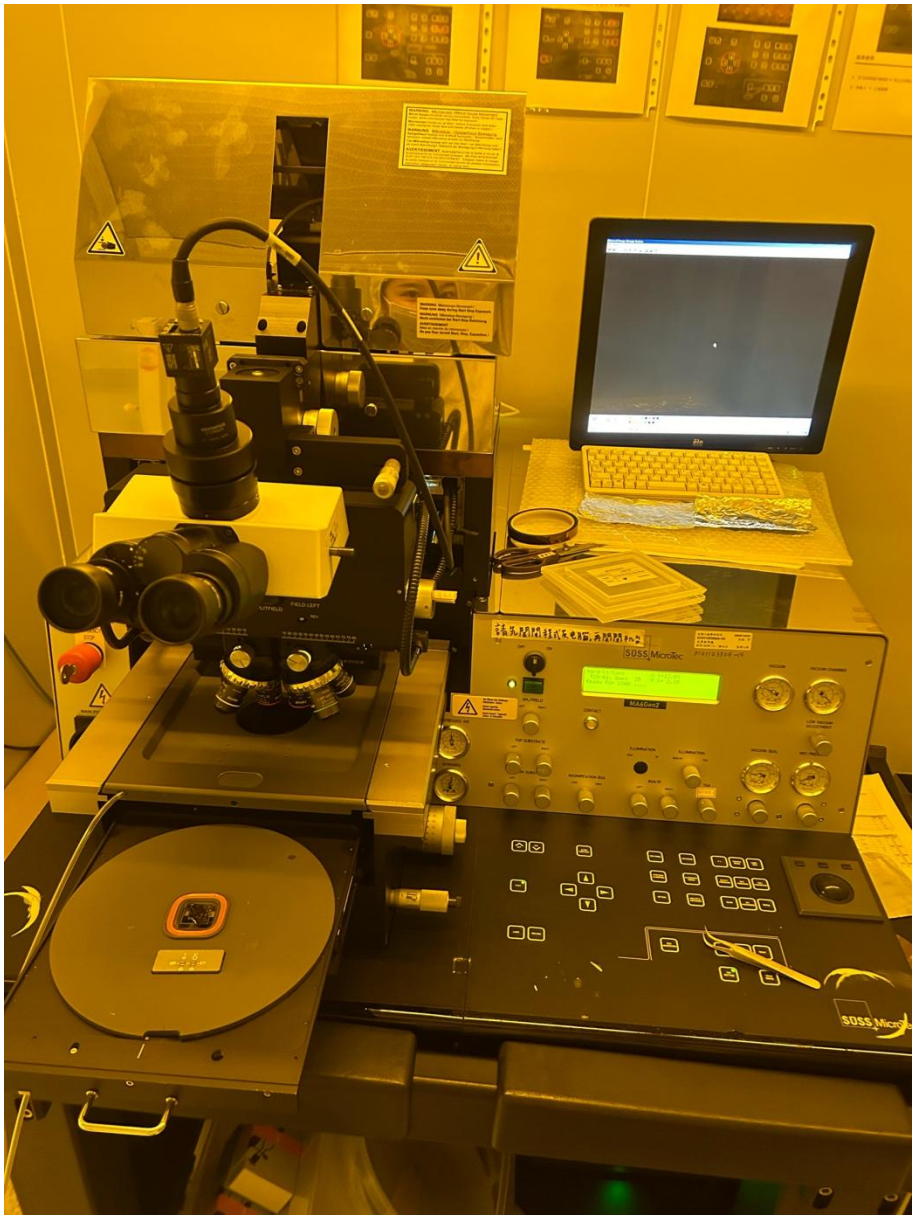

Figure 3.11 Mask aligner

doi:10.6342/NTU202500081

3.3.9 E-beam Evaporator and Thermal Evaporator

Electron beam evaporation is a type of physical vapor deposition (PVD) technique. It employs an electromagnetic field to precisely direct high-energy electrons onto a target material within a crucible, causing it to melt and deposit onto a substrate. In our experiment, we adjust parameters such as the Z-ratio, density, tooling, and current to deposit various metals.

Figure 3.12 E-beam evaporator and thermal evaporator

3.3.10 Solar Simulator

We use the WACOM WXS1555-L2 solar simulator for measuring light IV characteristics.

doi:10.6342/NTU202500081

This class AAA solar simulator features white light illumination and is equipped with both a xenon lamp and a halogen lamp.

Figure 3.13 Solar simulator

doi:10.6342/NTU202500081

Chaptor 4 Analysis of Solar Cell

Figure 4.1and 4.2 shows the two types of devices we fabricated: one with only SiO2 and the other with both Al2O3 and SiO2. Each type comes in three different sizes and four distinct shapes. In this section, Table 4.1 and 4.2 shows the parameters of the two types of devices with a size of 2000 μm.Table 4.3 shows the geometry of our devices.We will analyze the fundamental characteristics of these devices and examine how these properties change after adding quantum dot photoresist (QDPR).

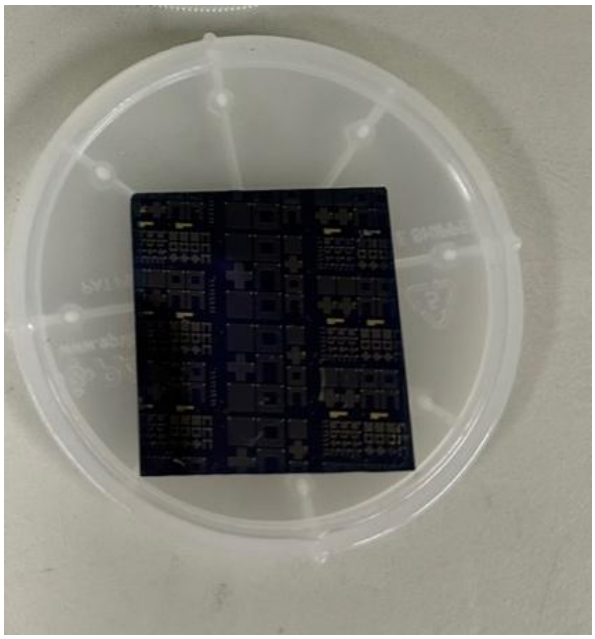

Figure 4.1 PECVD only

doi:10.6342/NTU202500081

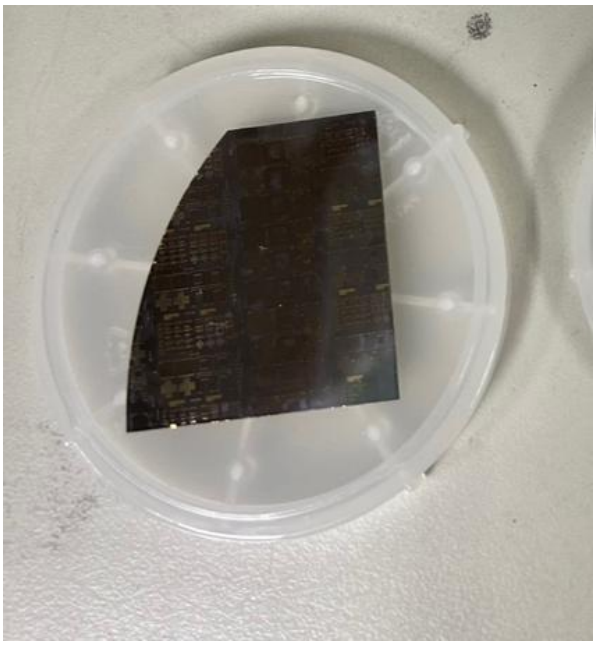

Figure 4.2 PECVD+ALD

Table 4.1 Parameter of PECVD only

PECVD	V_{oc}(V)	Jsc(mA/cm^2)	FF	PCE(%)
SQUARE 2000	1.01	15.5	0.83	13.2
HOLLOW	0.96	13.6	0.82	10.7
CROSS	0.96	13.4	0.84	10.9
U-SHAPE	0.93	14.4	0.79	10.7

doi:10.6342/NTU202500081

Table 4.2 Parameter of ALD+PECVD

ALD	V_{oc}(V)	Jsc(mA/cm^2)	FF	PCE(%)
SQUARE 2000	1.00	14.5	0.82	12.0
HOLLOW	0.98	14.5	0.79	11.3
CROSS	0.99	14.8	0.81	12.0
U-SHAPE	0.99	14.7	0.80	11.6

Table 4.3 Geometry of our devices

Size(um)		square	hollow square	cross-shape	U-shape
3000	Area(cm2)	0.0843	0.0589	0.0452	0.0529
	perimeter(cm)	1.2	1.8	1.2	1.6
2000	Area(cm2)	0.0362	0.0265	0.0218	0.0219
	perimeter(cm)	0.8	1.2	0.8	1.1
1000	Area(cm2)	0.008	0.0058	0.0051	0.0049
	perimeter(cm)	0.4	0.6	0.4	0.55

4.1 Current density

Figures 4.3 and 4.4 show the I-V curves of four types of devices with dimensions of 2000 μm, fabricated using PECVD and ALD+PECVD, respectively. Due to ALD's improved interface quality and passivation of surface defects, the devices become more stable, and the Jsc of ALD-treated devices exceeds 14 mA/cm².

doi:10.6342/NTU202500081

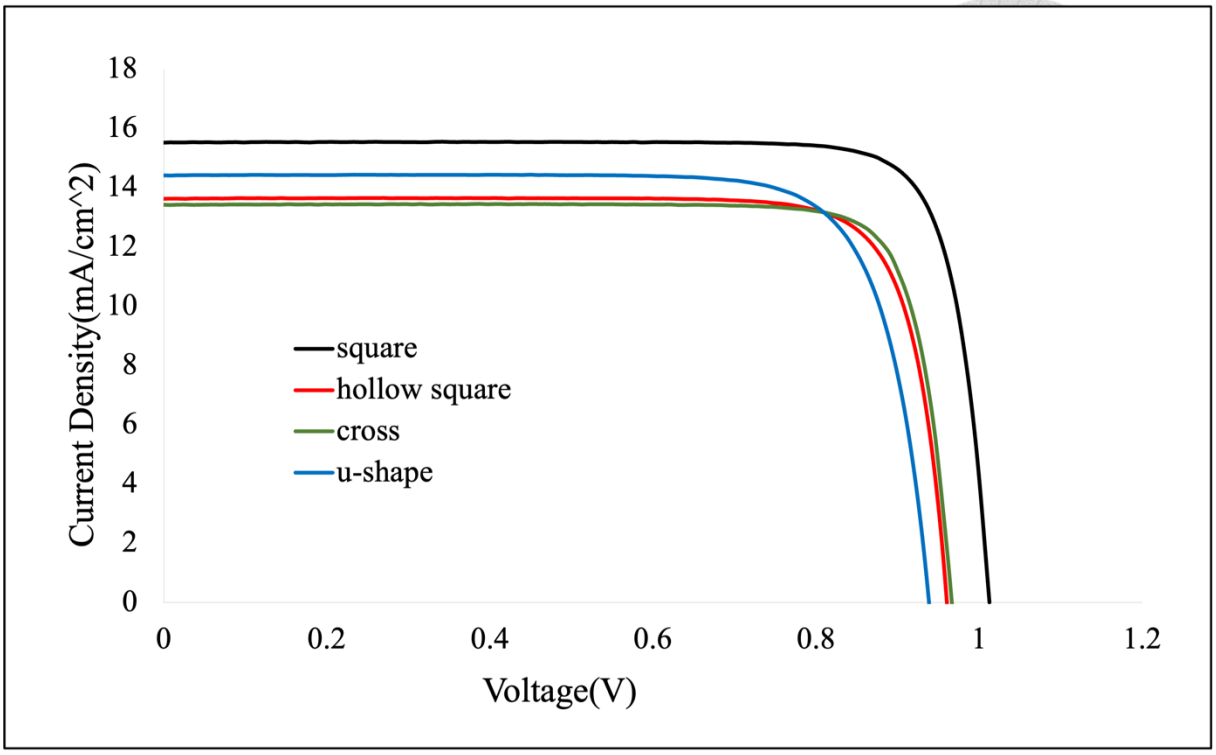

Figure 4.3 PECVD 2000um IV curve

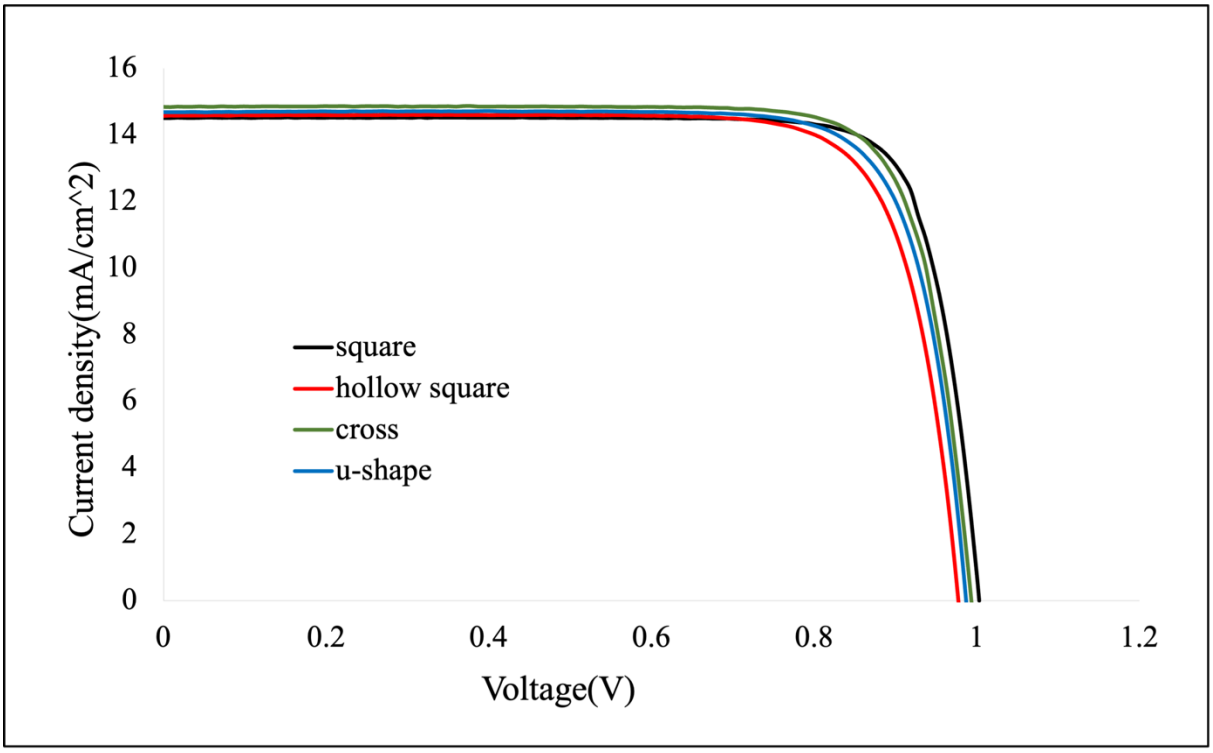

Figure 4.4 ALD 2000um IV curve

4.2 Dark Current

Figures 4.5 and 4.6 show the Dark Current of four types of devices with dimensions of

doi:10.6342/NTU202500081

2000 μm, fabricated using PECVD and ALD+PECVD, respectively. Figures 4.7, 4.8, and 4.9 show the dark current density at -5V. It can be observed that devices with ALD + PECVD exhibit lower leakage current compared to devices with only PECVD. Figure 4.10 shows the plot of dark current density at -5V versus the perimeter-to-area ratio, comparing the devices I fabricated with the lab's previous work. From equation 4.1 to 4.3, the leakage current of the device consists of the dark current from the bulk and the side. The side leakage current is influenced by the perimeter-to-area (P/A) ratio. From the devices I fabricated, the trend aligns with the observation that devices with a larger P/A ratio exhibit a significant increase in leakage current.[18, 24, 25]

$$J_d = J_b + J_p \quad \text{Equation(4.1)}$$

$$J_b = J_{b0} \exp\left(\frac{V - J_d \times A \times R_s}{n_b V_t}\right) \quad \text{Equation (4.2)}$$

$$J_p = q \frac{n_s p_s - n_i^2}{(n_s + n_l)/S_{p0} + (p_s + p_l)/S_{n0}} \times d \times \frac{P}{A} \quad \text{Equation (4.3)}$$

doi:10.6342/NTU202500081

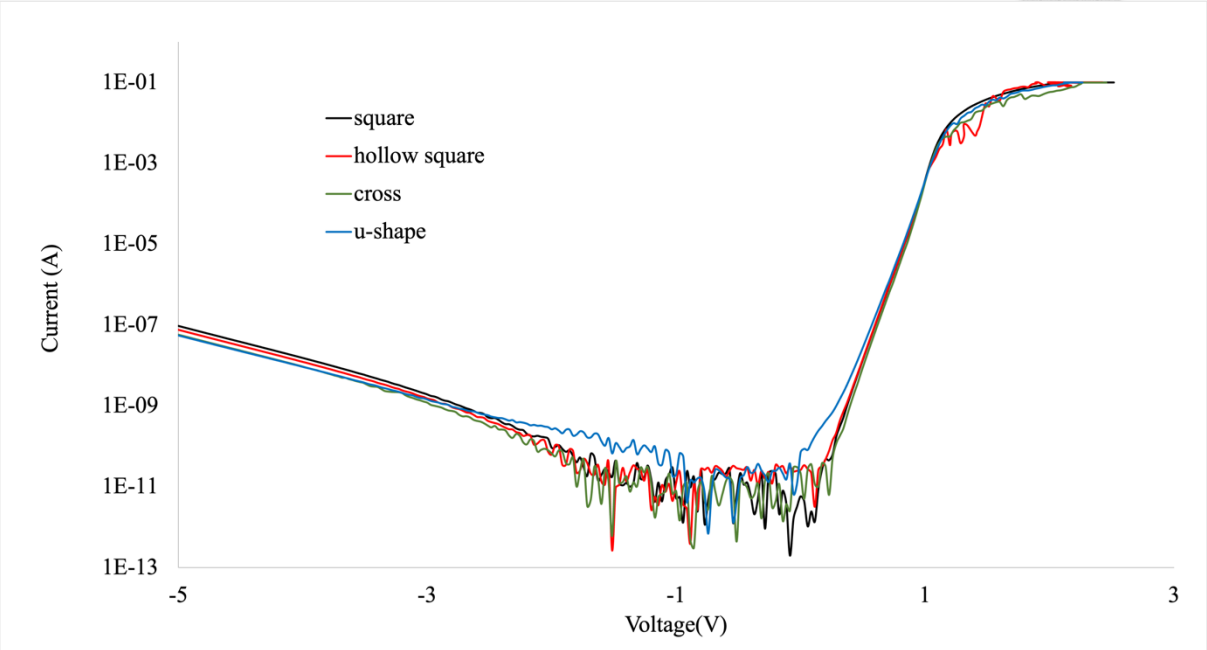

Figure 4.5 PECVD 2000um Dark Current

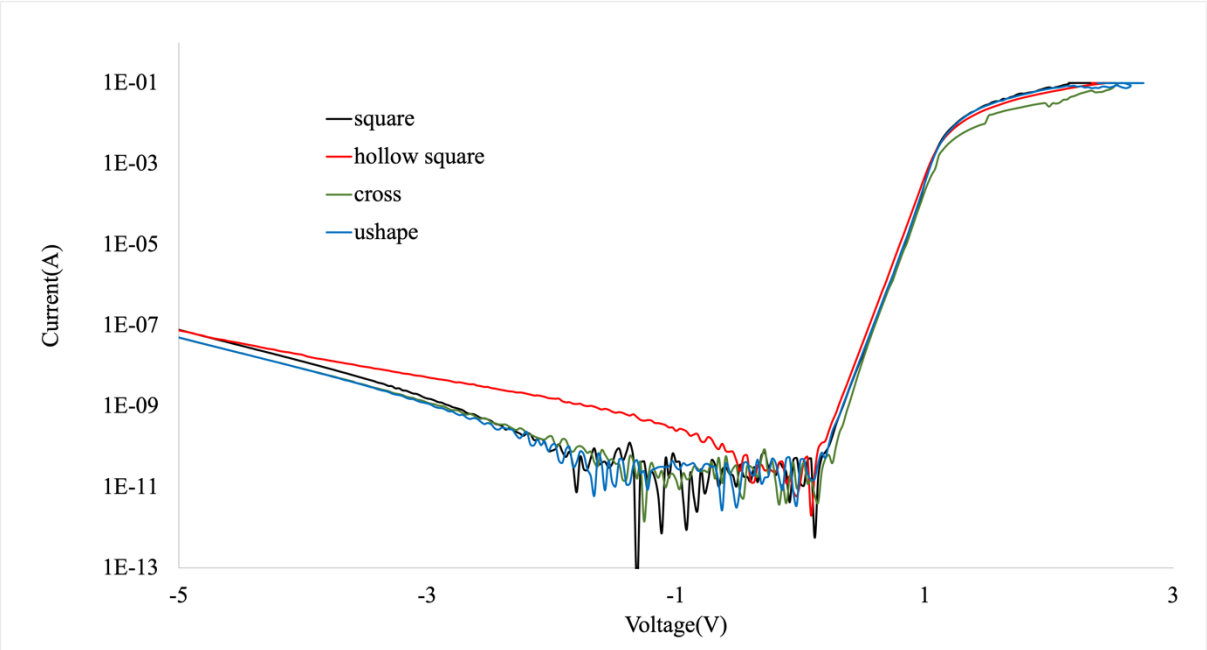

Figure 4.6 ALD+PECVD 2000um Dark Current

doi:10.6342/NTU202500081

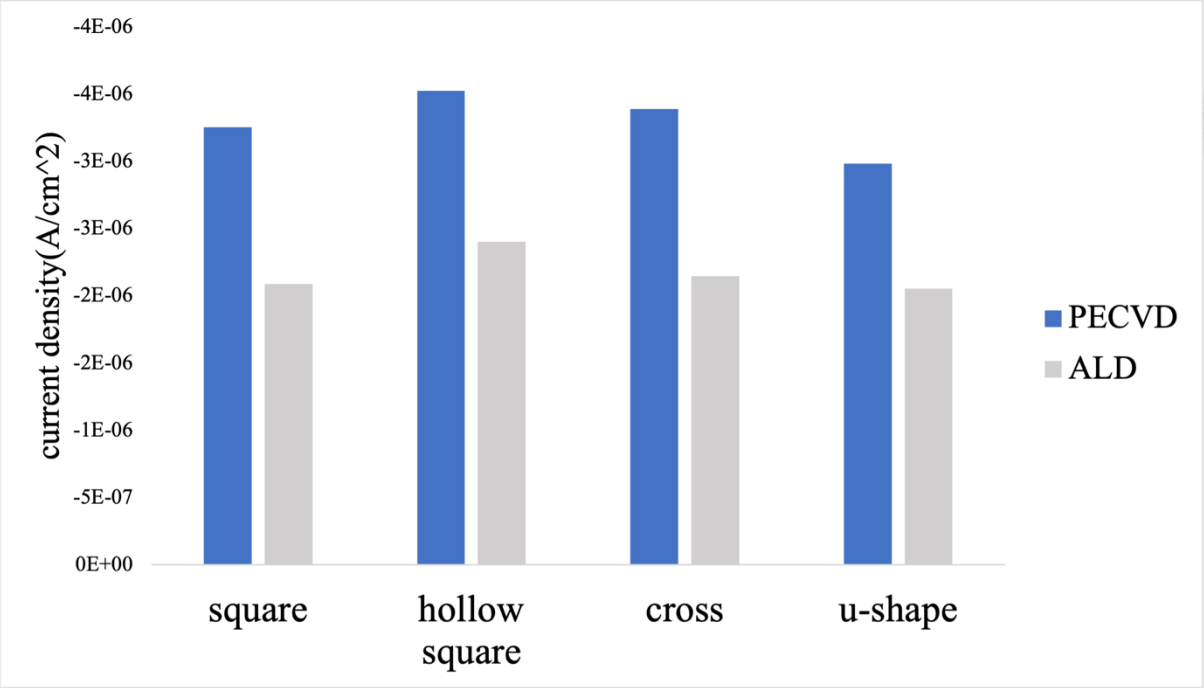

Figure 4.7 Dark current density at -5V of 3000um devices comparison

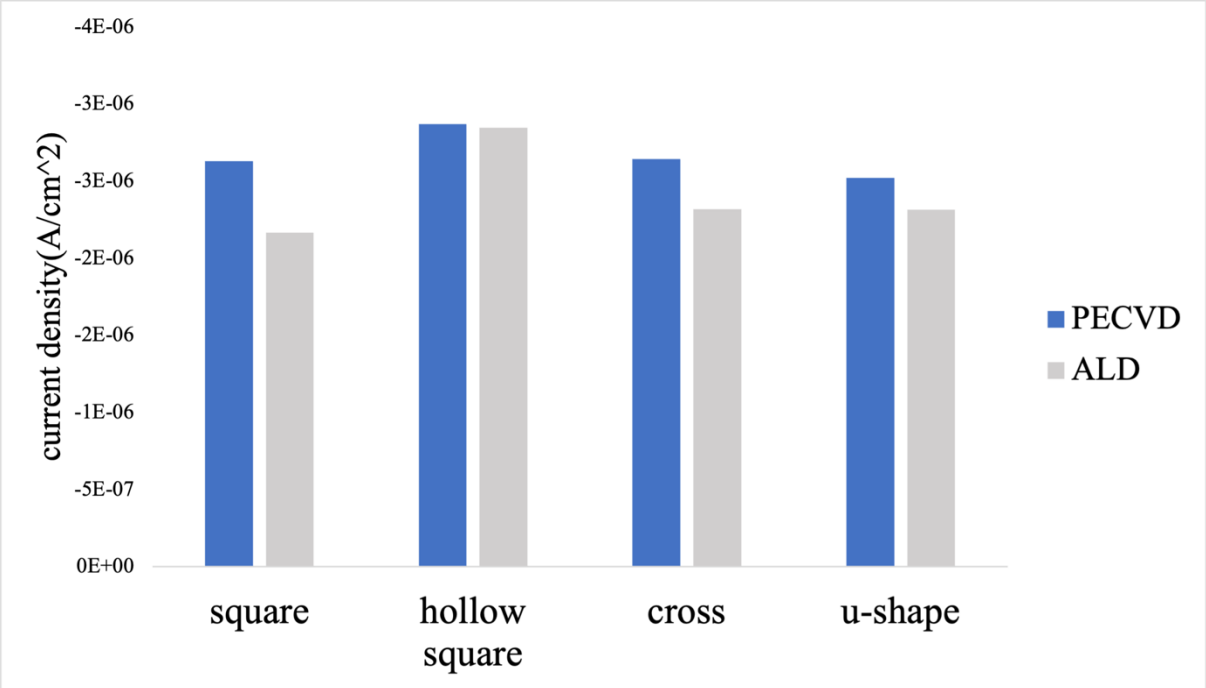

Figure 4.8 Dark current density at -5V of 2000um devices comparison

doi:10.6342/NTU202500081

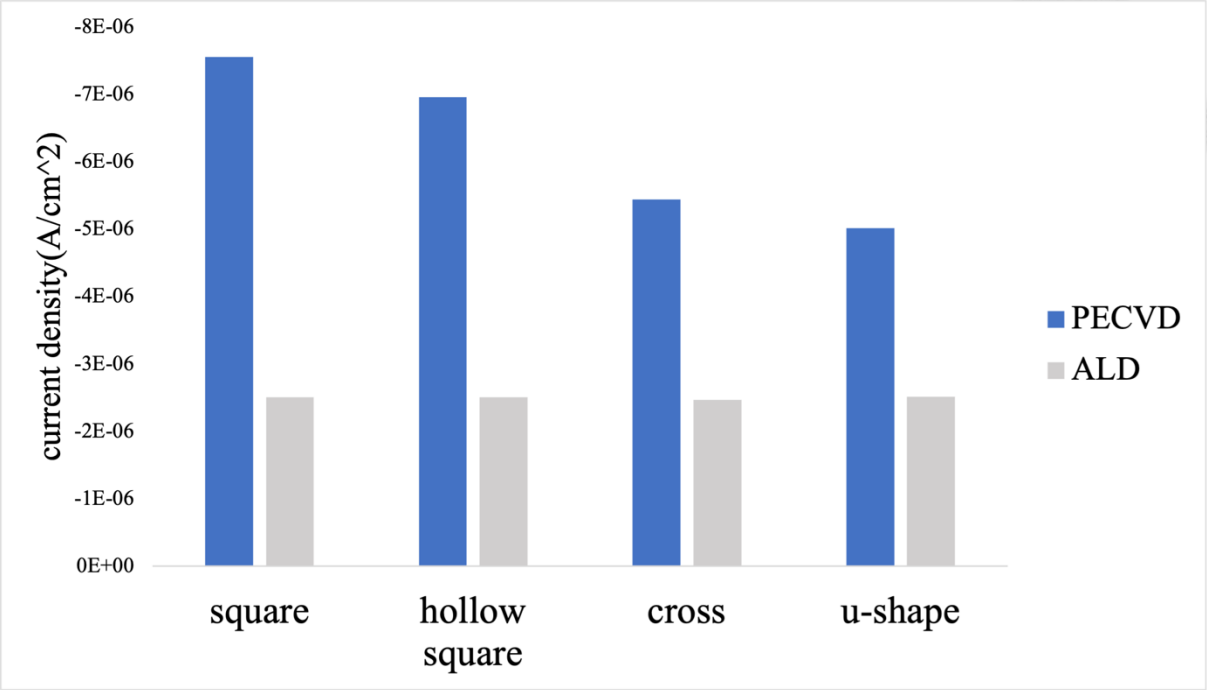

Figure 4.9 Dark current density at -5V of 1000um devices comparison

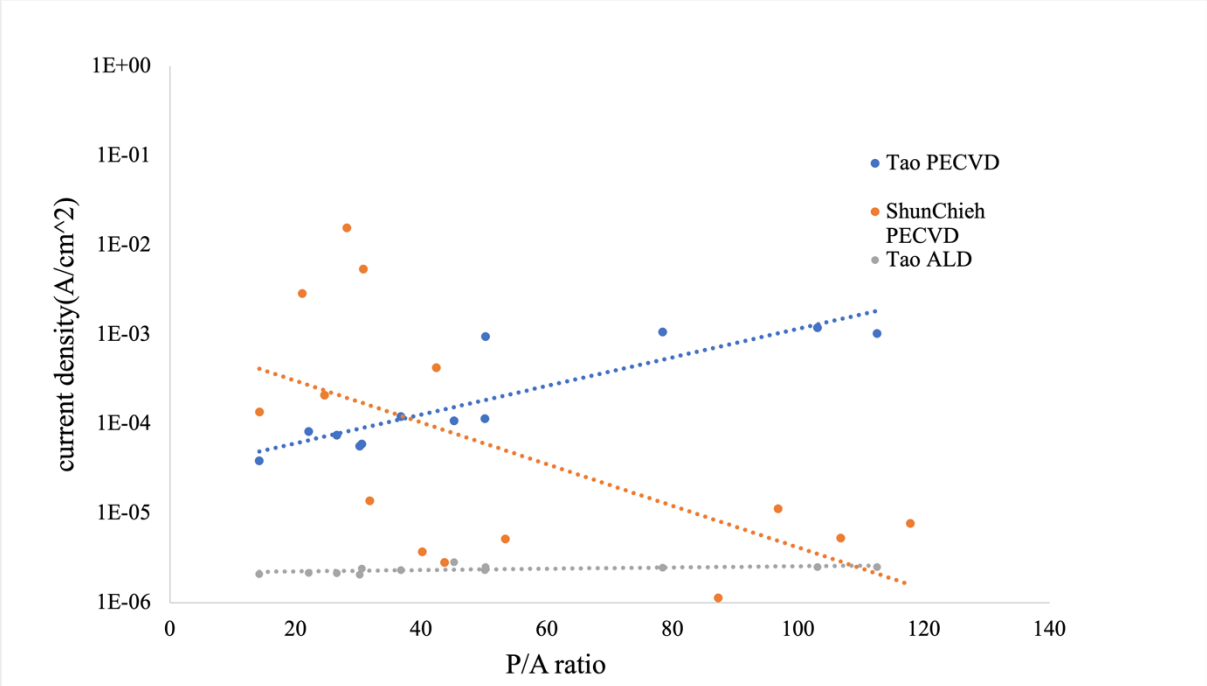

Figure 4.10 Dark current-P/A ratio comparison

4.3 Solar Cell with QDPR

In the past, we attempted various methods to apply quantum dots onto devices, such as

doi:10.6342/NTU202500081

direct drop-casting and mixing them with PDMS, each with its own set of challenges. This time, we used QDPR to achieve better sidewall coverage. By utilizing photolithography, QDPR was applied to the sides of the devices, and after hard baking, the height of the QDPR layer was approximately 2700 nm.

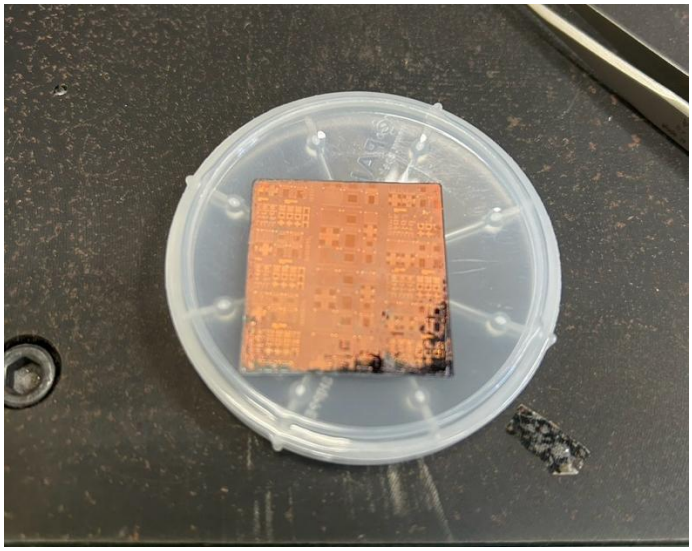

Figure 4.11 Devices with red QDPR

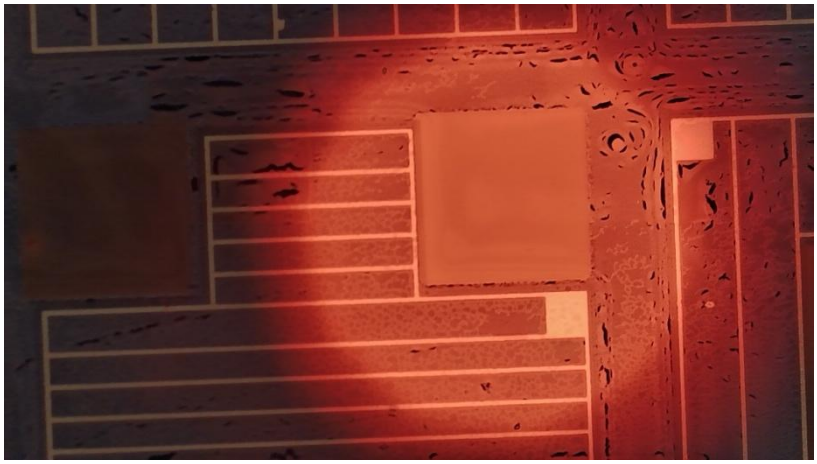

Figure 4.12 Devices with red QDPR under FLOM

doi:10.6342/NTU202500081

4.3.1 IV-curve

Figures 4.13 to 4.16 show the I-V curve changes for four types of 2000 μm PECVD devices after adding QDPR. We observe a trend of increased Jsc after the addition of QDPR. The hollow square shape exhibited the highest increase in Jsc, rising from 13.6 mA/cm² to 19.8 mA/cm², representing a 45% improvement.

Figures 4.17 to 4.20 show the I-V curve changes for four types of 2000 μm PECVD +ALD devices after adding QDPR. We also observe a trend of increased Jsc after the addition of QDPR. The cross shape exhibited the highest increase in Jsc, rising from 14.8 mA/cm² to 19.6 mA/cm², representing a 33% improvement.

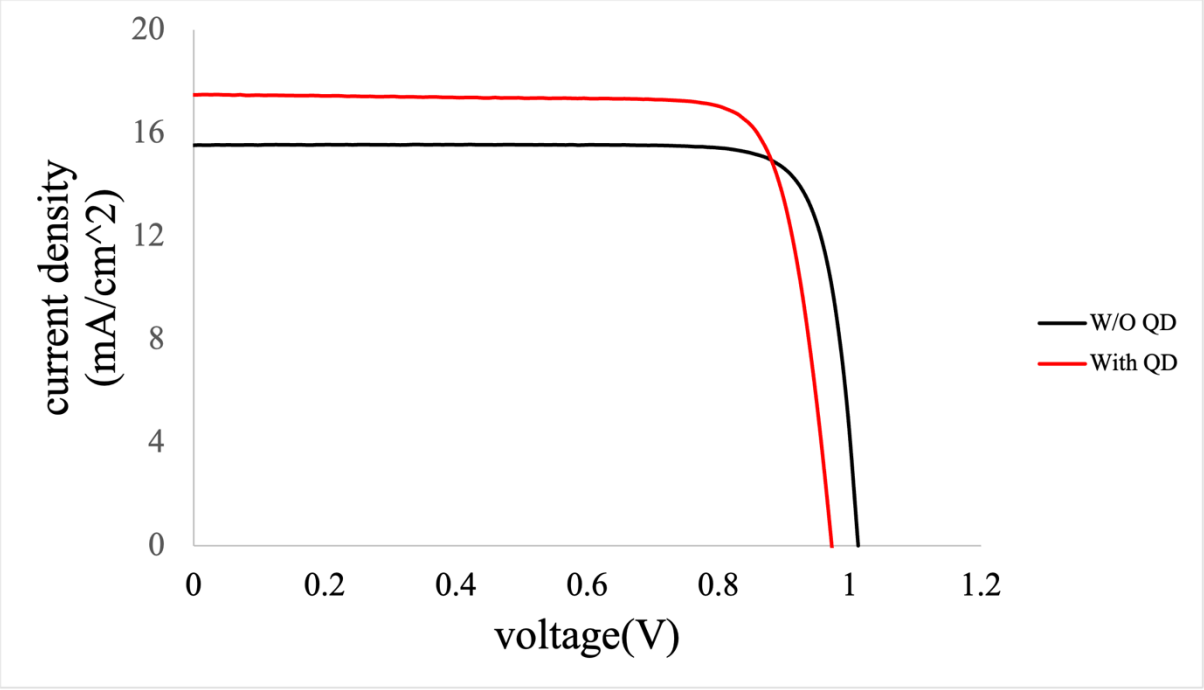

Figure 4.13 PECVD 2000um square IV-curve comparison

doi:10.6342/NTU202500081

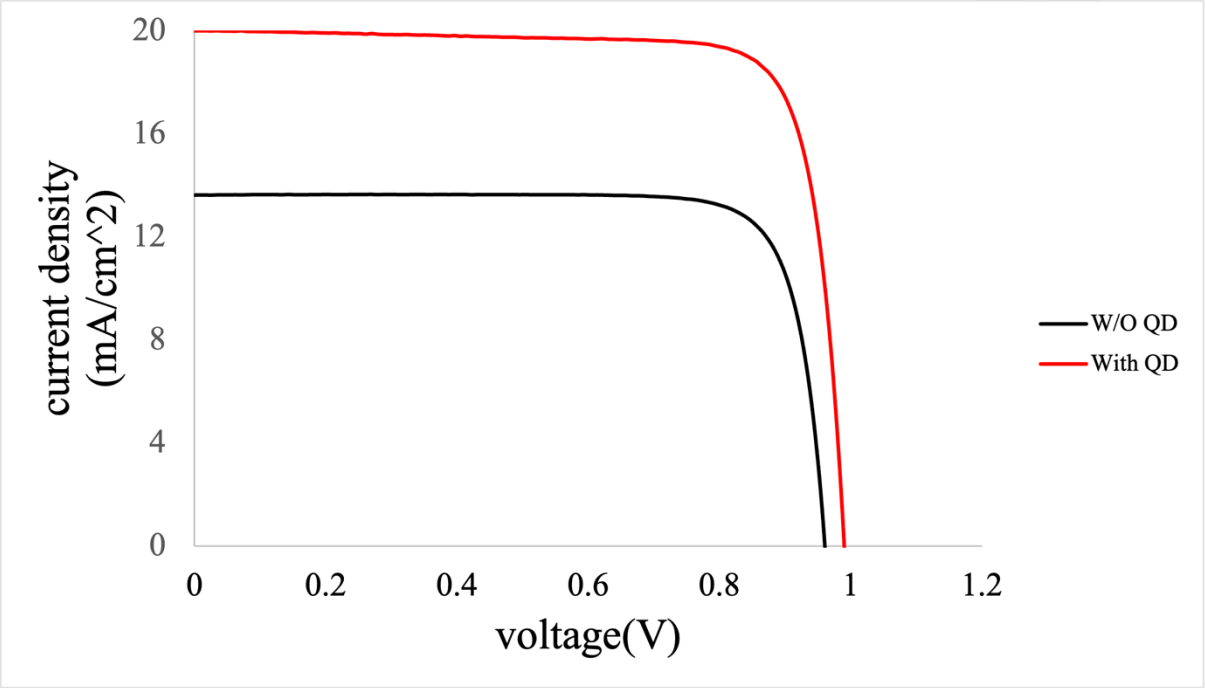

Figure 4.14 PECVD 2000um hollow square IV-curve comparison

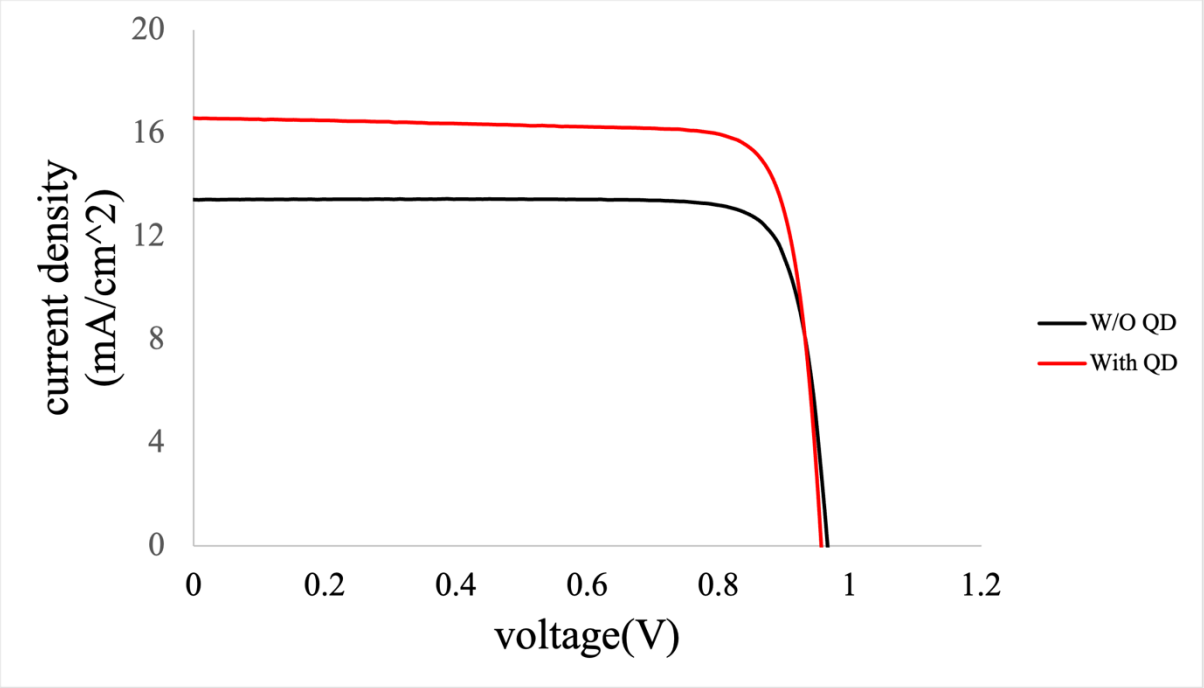

Figure 4.15 PECVD 2000um cross IV-curve comparison

doi:10.6342/NTU202500081

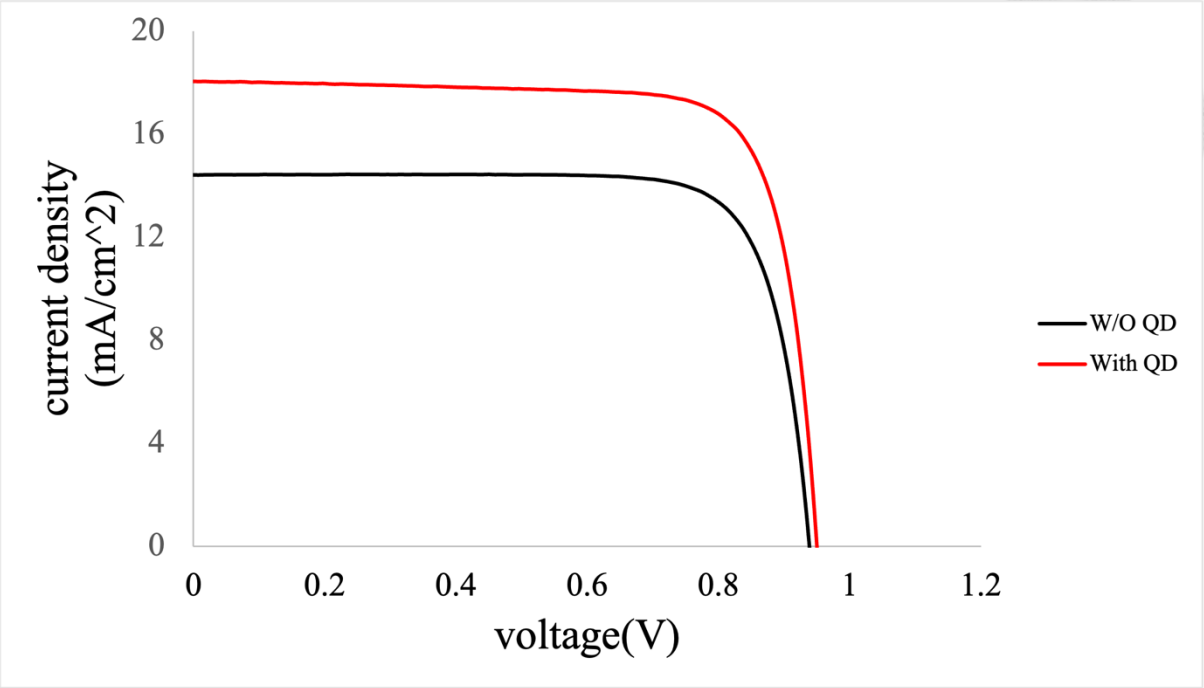

Figure 4.16 PECVD 2000um U-shape IV-curve comparison

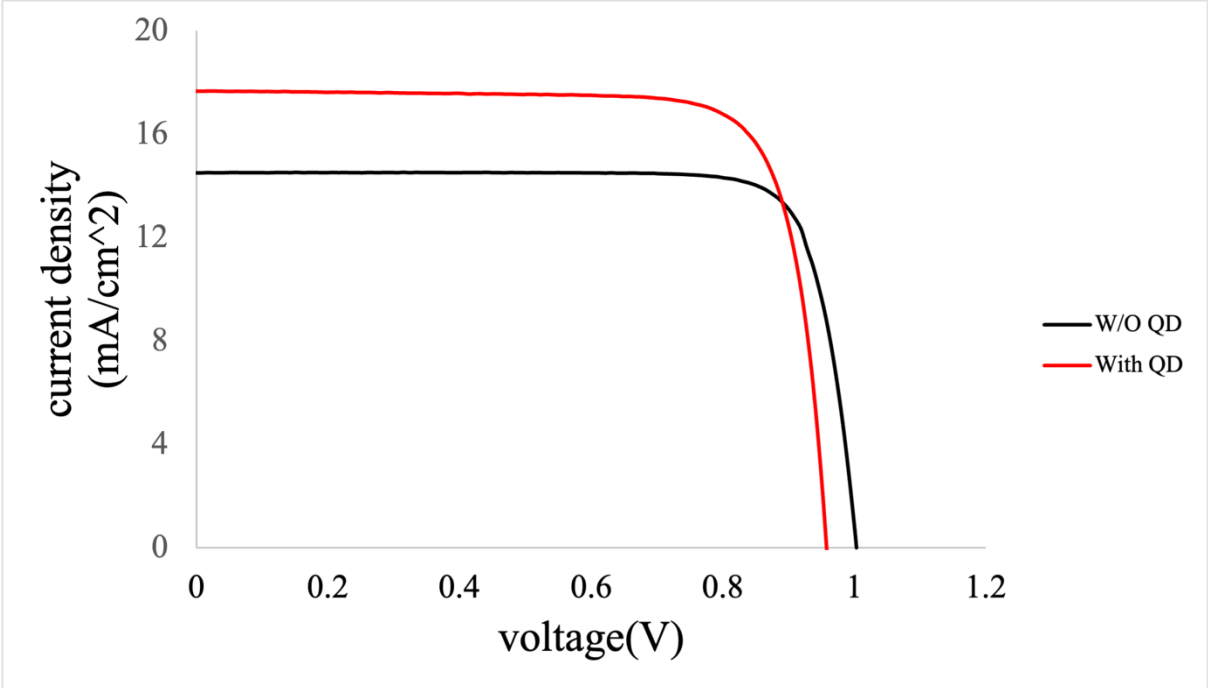

Figure 4.17 ALD 2000um square IV-curve comparison

doi:10.6342/NTU202500081

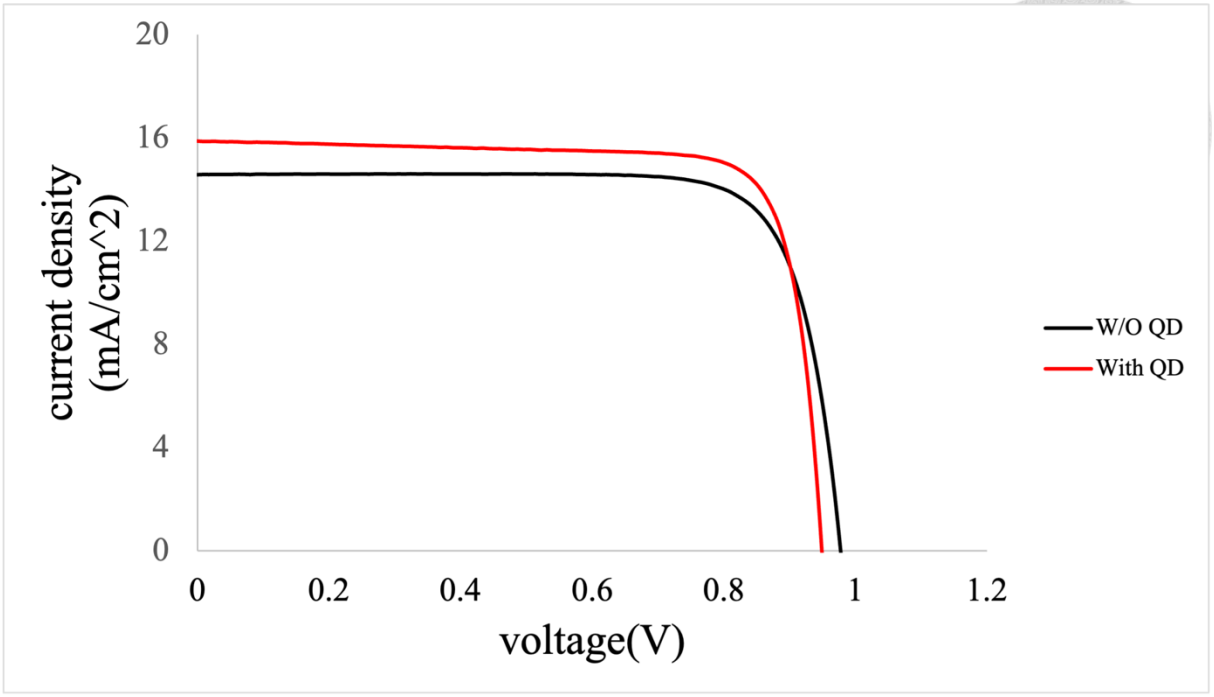

Figure 4.18 ALD 2000um hollow square IV-curve comparison

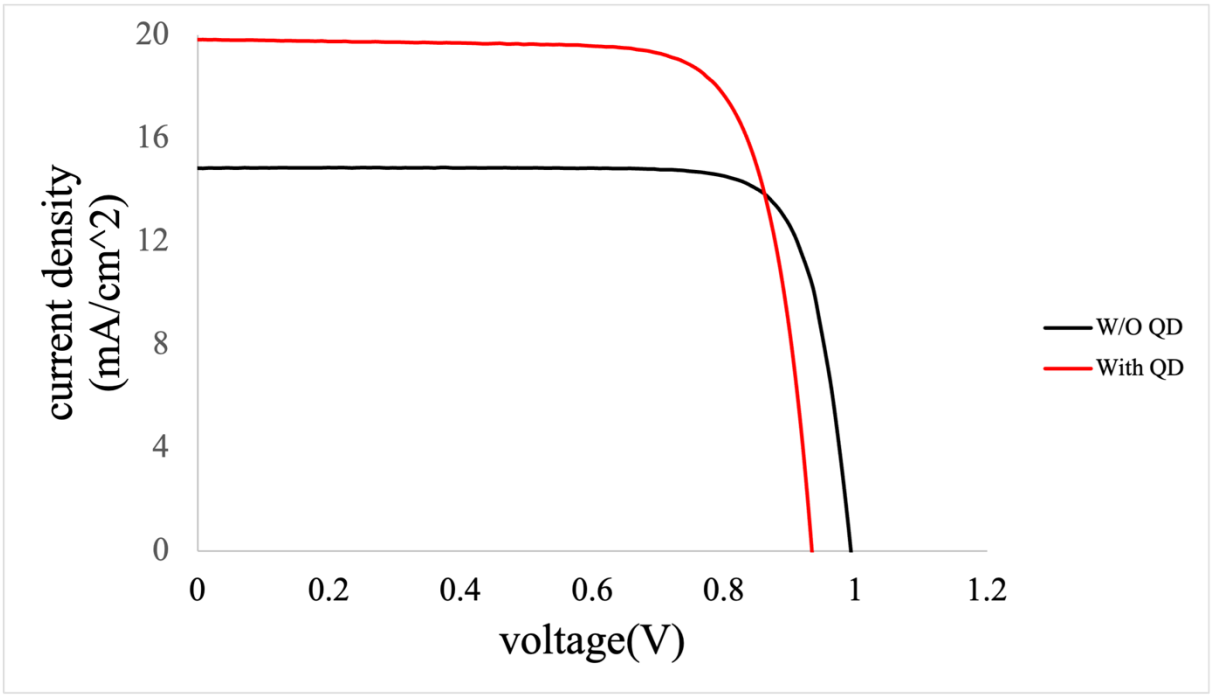

Figure 4.19 ALD 2000um cross IV-curve comparison

doi:10.6342/NTU202500081

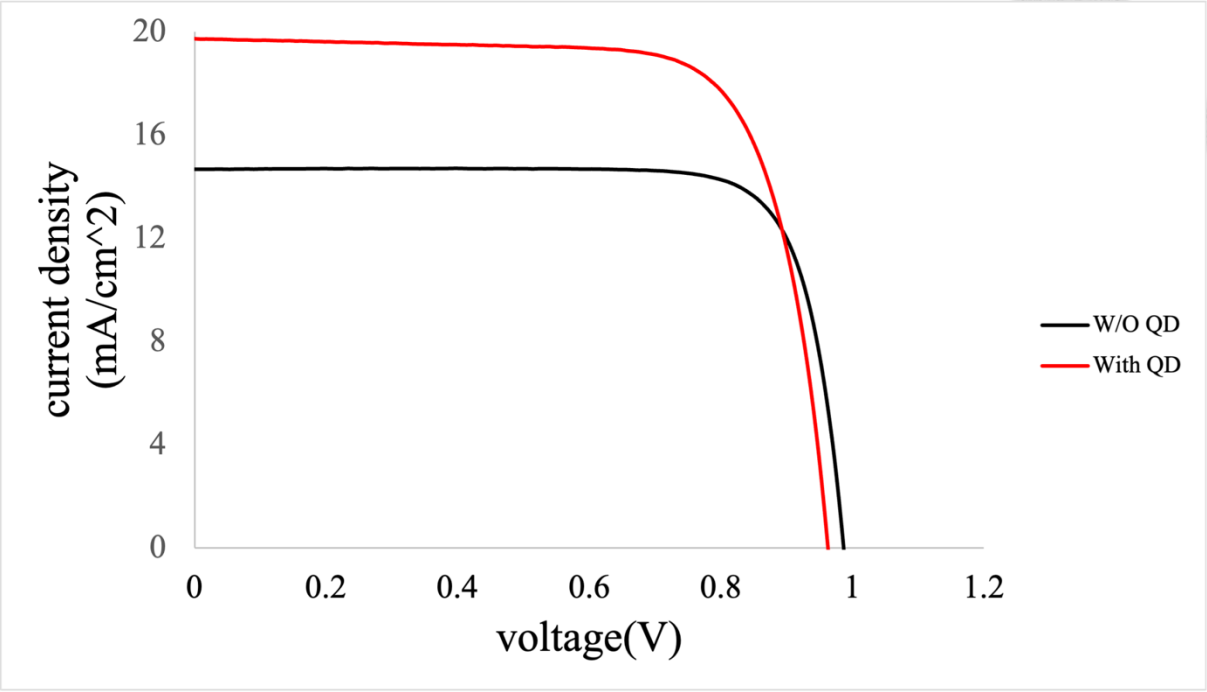

Figure 4.20 ALD 2000um U-shape IV-curve comparison

4.3.2 EQE

As expected, alongside the increase in Jsc, there is also a trend of increased EQE. Figures 4.21 to 4.24 show the EQE curve changes for four types of 2000 μm PECVD devices after adding QDPR. Figures 4.25 to 4.28 show the EQE curve changes for four types of 2000 μm ALD+PECVD devices after adding QDPR.

doi:10.6342/NTU202500081

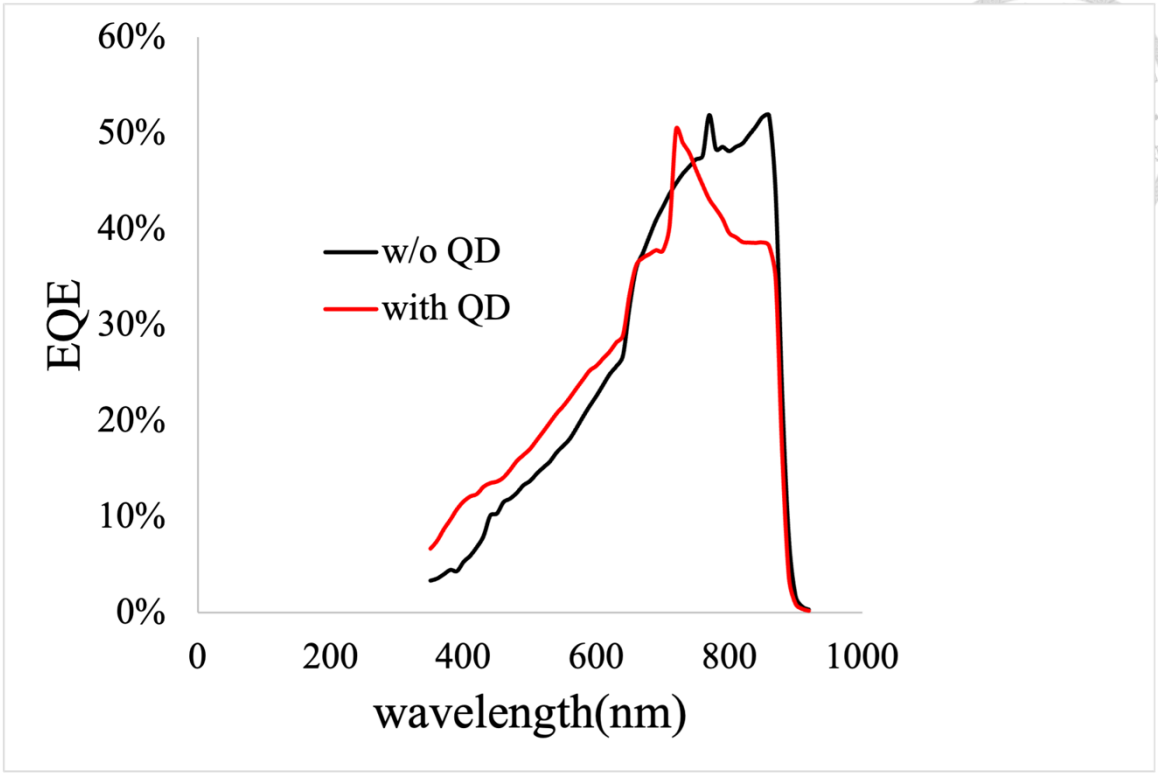

Figure 4.21 PECVD 2000um square EQE comparison

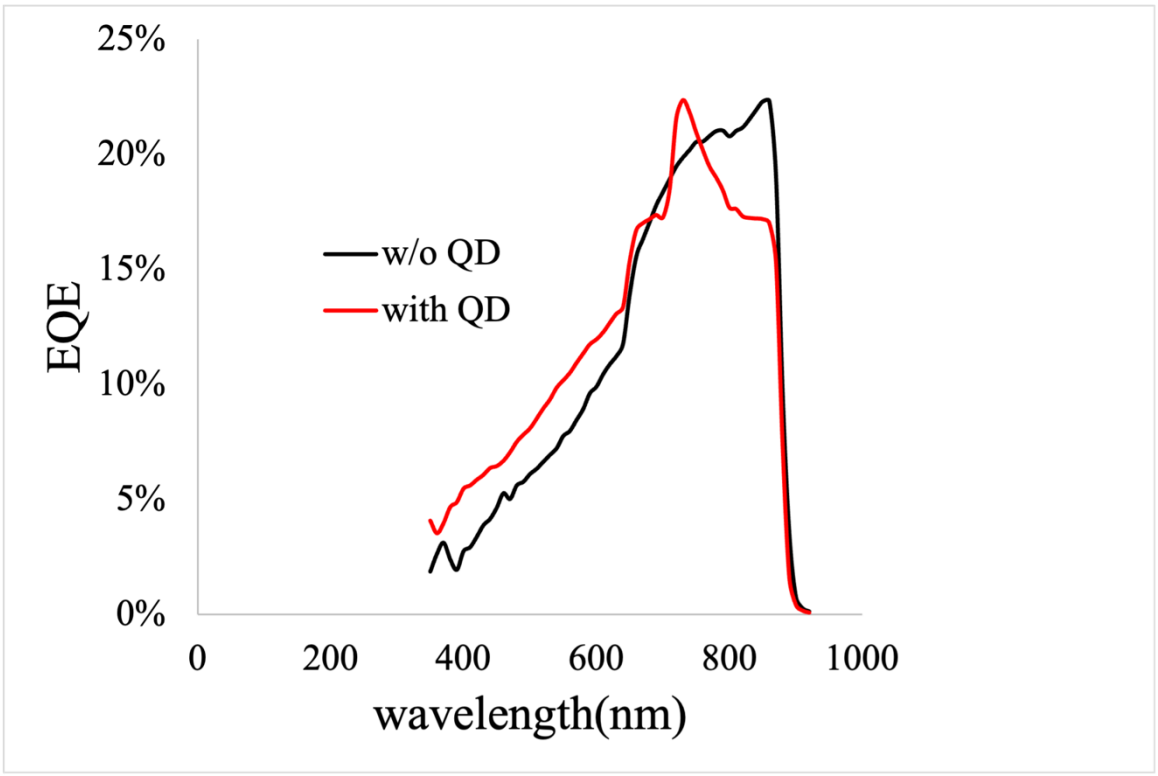

Figure 4.22 PECVD 2000um hollow square EQE comparison

doi:10.6342/NTU202500081

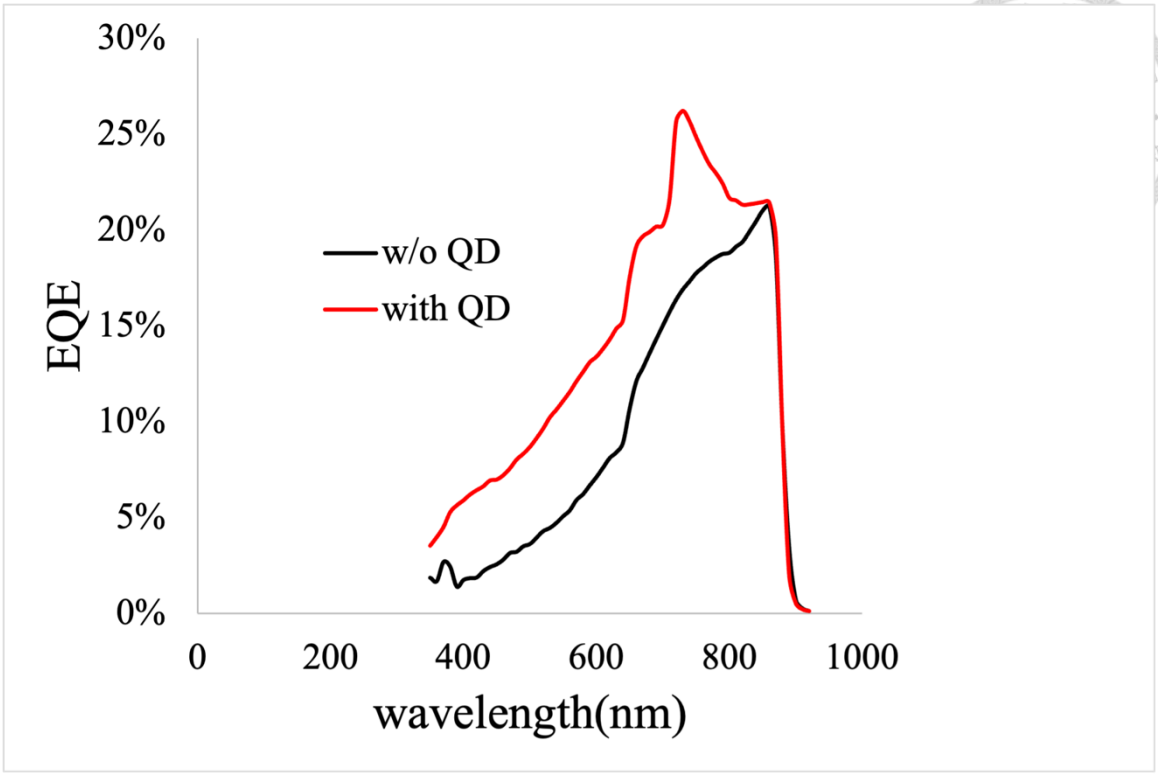

Figure 4.23 PECVD 2000um cross EQE comparison

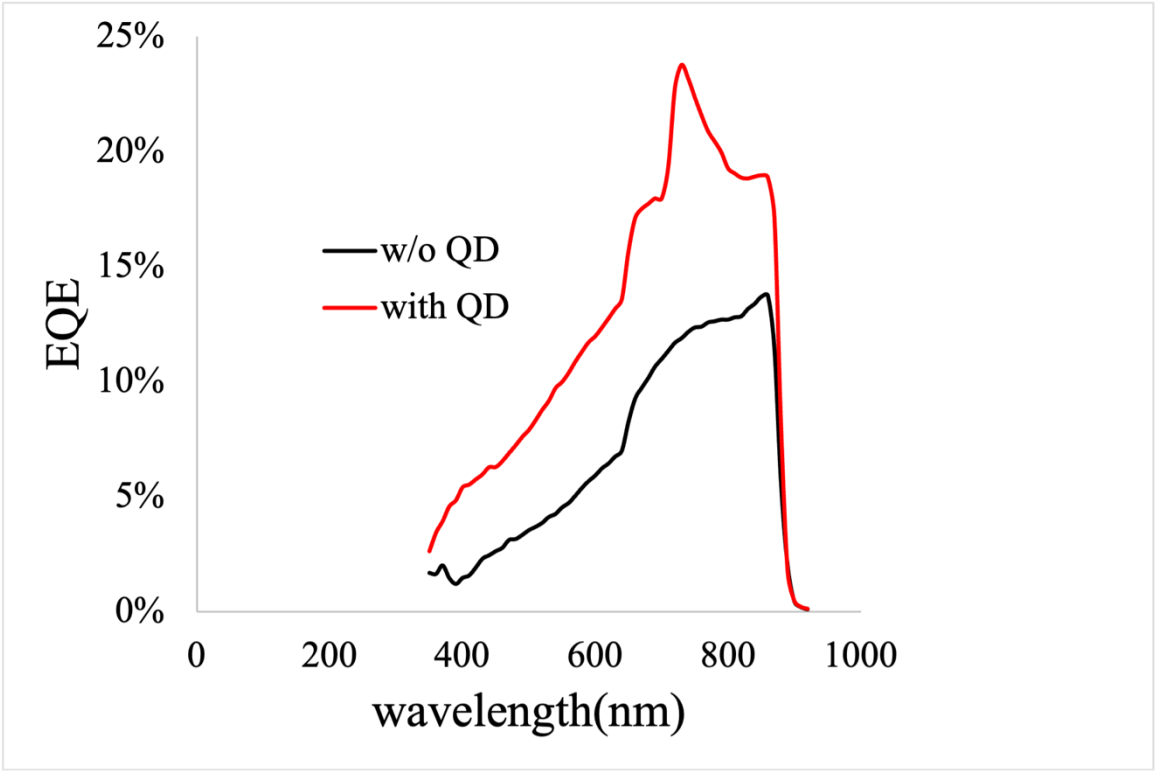

Figure 4.24 PECVD 2000um U-shape EQE comparison

doi:10.6342/NTU202500081

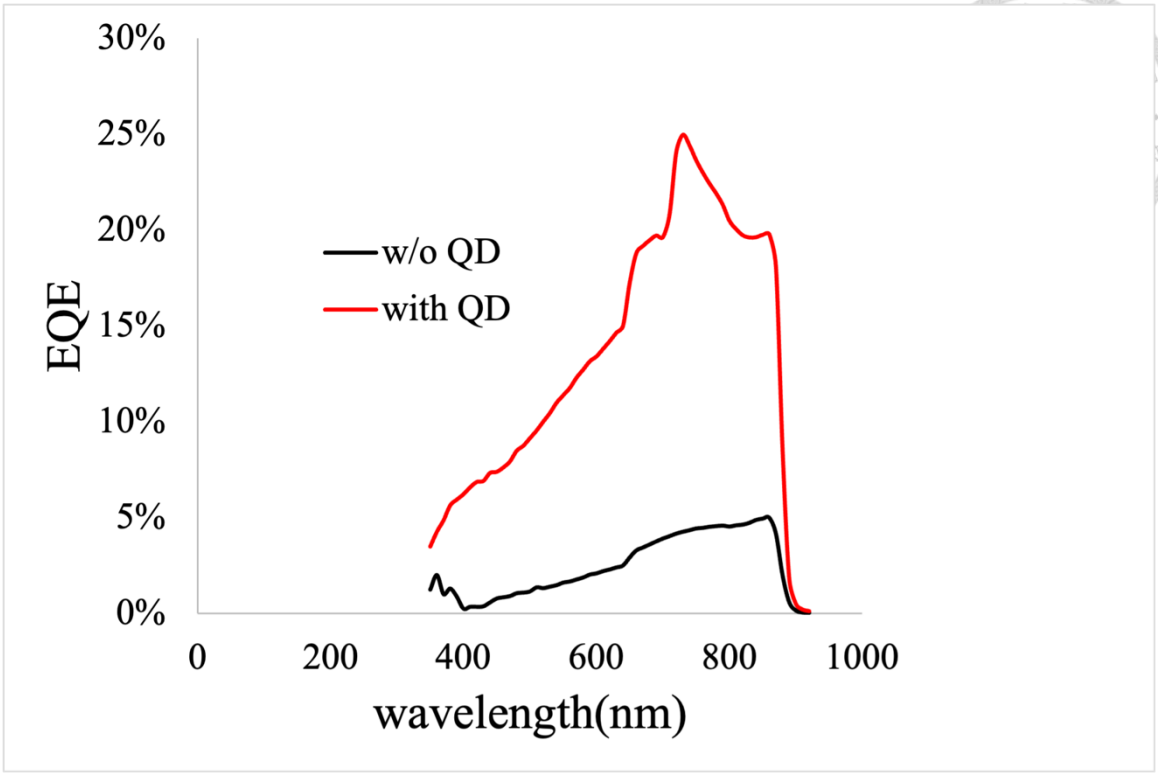

Figure 4.25 ALD 2000um square EQE comparison

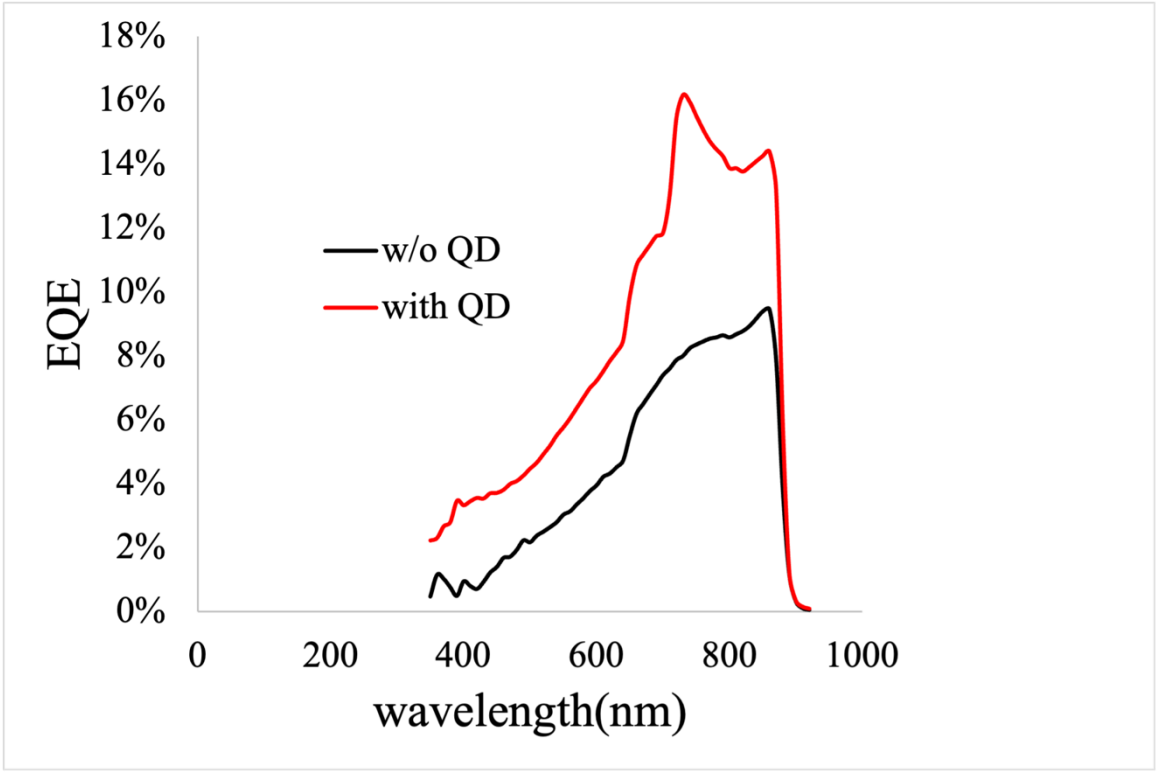

Figure 4.26 ALD 2000um hollow square EQE comparison

doi:10.6342/NTU202500081

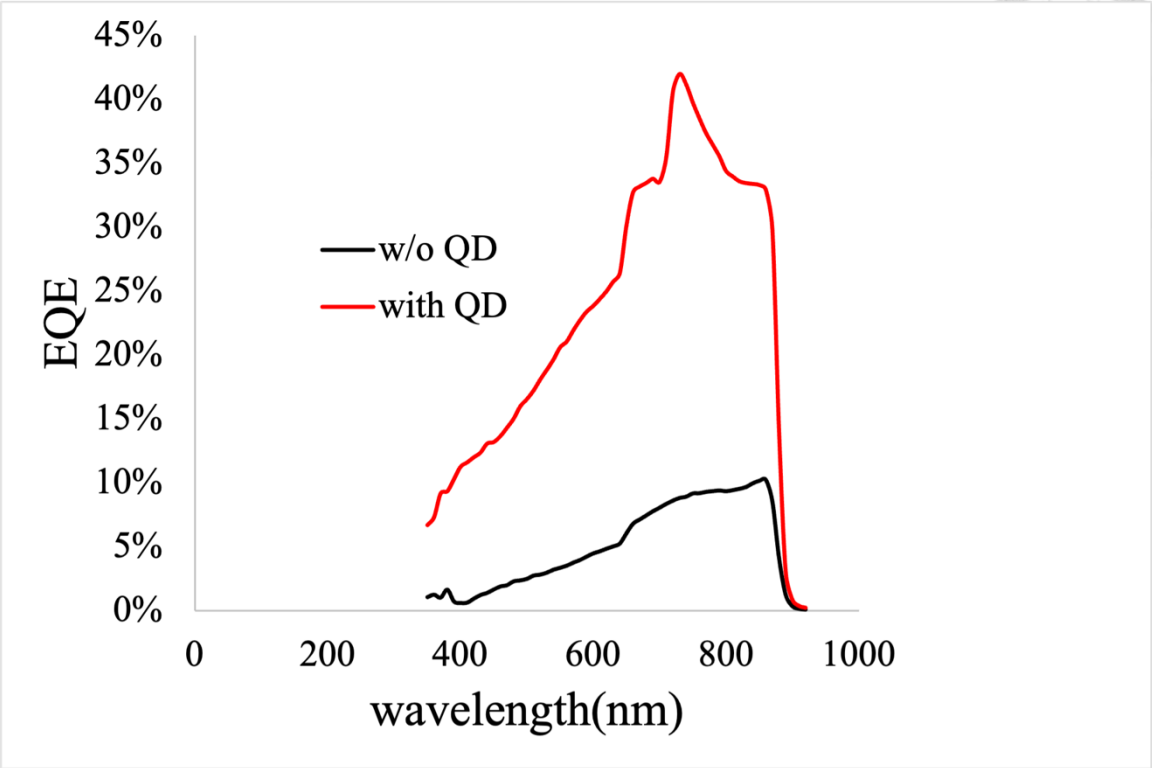

Figure 4.27 ALD 2000um cross EQE comparison

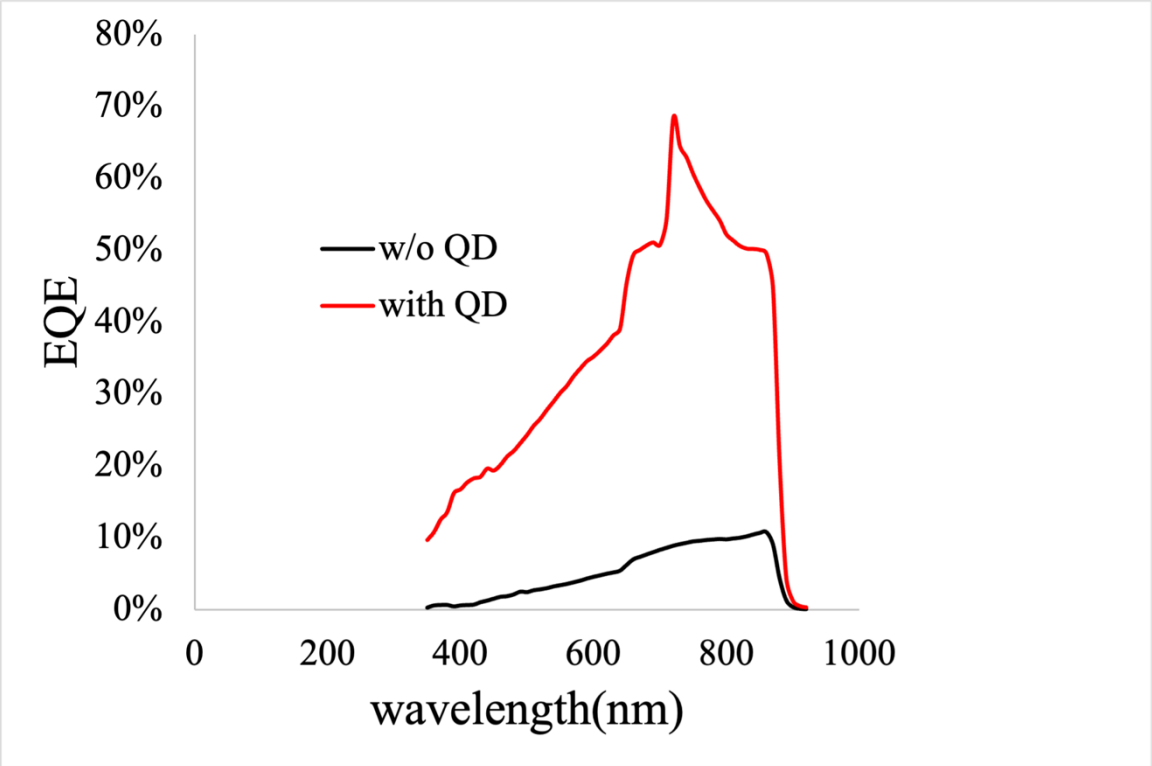

Figure 4.28 ALD 2000um U-shape EQE comparison

doi:10.6342/NTU202500081

4.3.3 Fill Factor

We observed a general trend of decreased fill factor after adding QDPR, which we speculate is due to The addition of quantum dots (QDs) can reduce the fill factor (FF) in depleted-heterojunction QDSCs because of the formation of a Schottky barrier at the QD/metal electrode interface. This barrier increases carrier recombination and impedes hole extraction.[26]

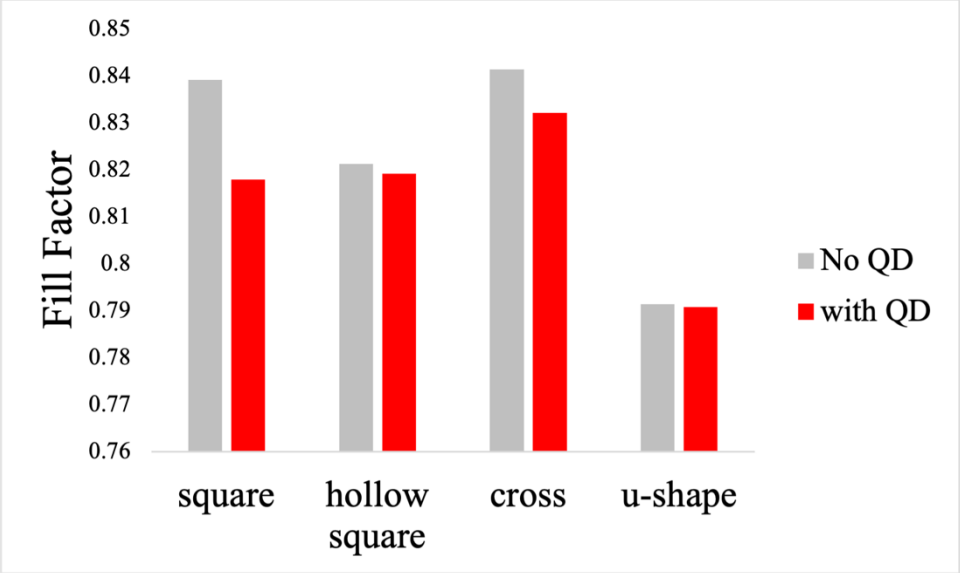

Figure 4.29 PECVD 2000um fill factor comparison

doi:10.6342/NTU202500081

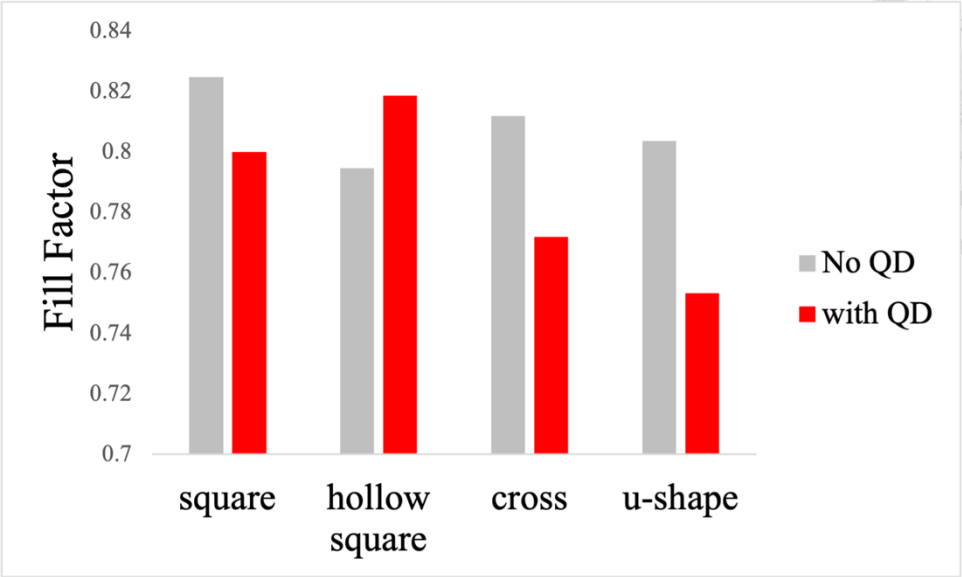

Figure 4.30 ALD 2000um fill factor comparison

4.3.4 Series Resistance

We observed a general trend of increased series resistance after adding QDPR, which we speculate is due to

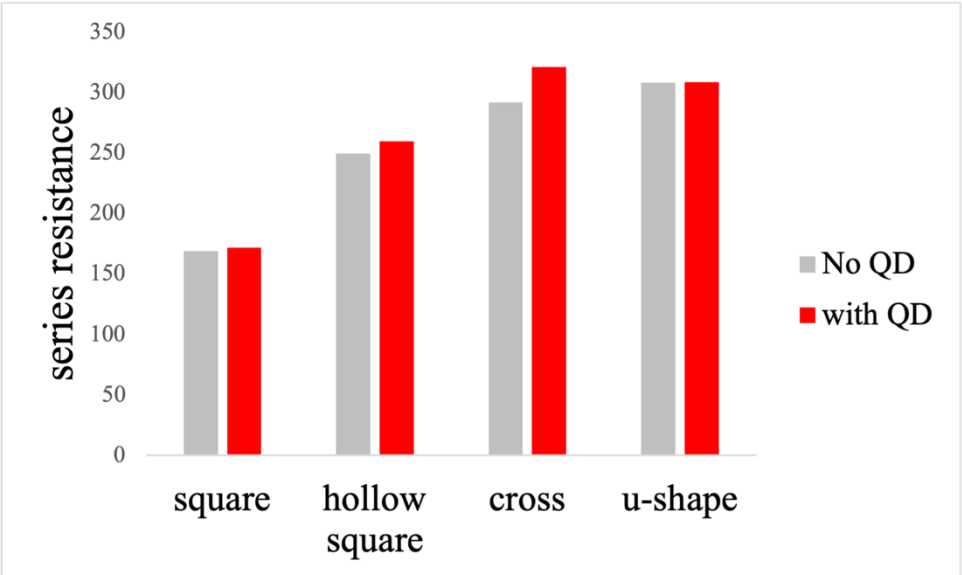

Figure 4.31 PECVD 2000um series resistance comparison

doi:10.6342/NTU202500081

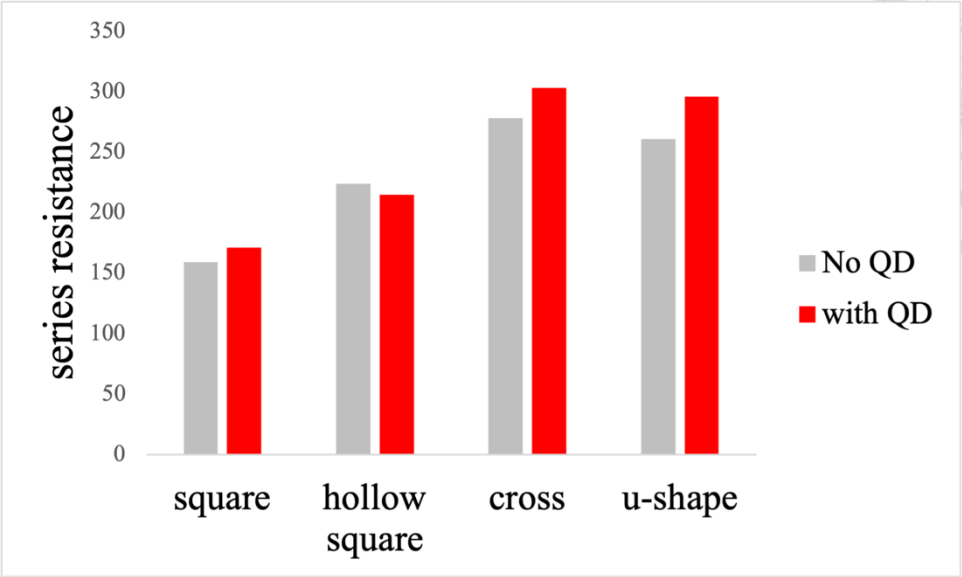

Figure 4.32ALD 2000um series resistance comparison

4.3.5 Ideality Factor

The ideality factor generally falls between 1.5 and 2, and we observed an decreasing trend after adding QDPR.

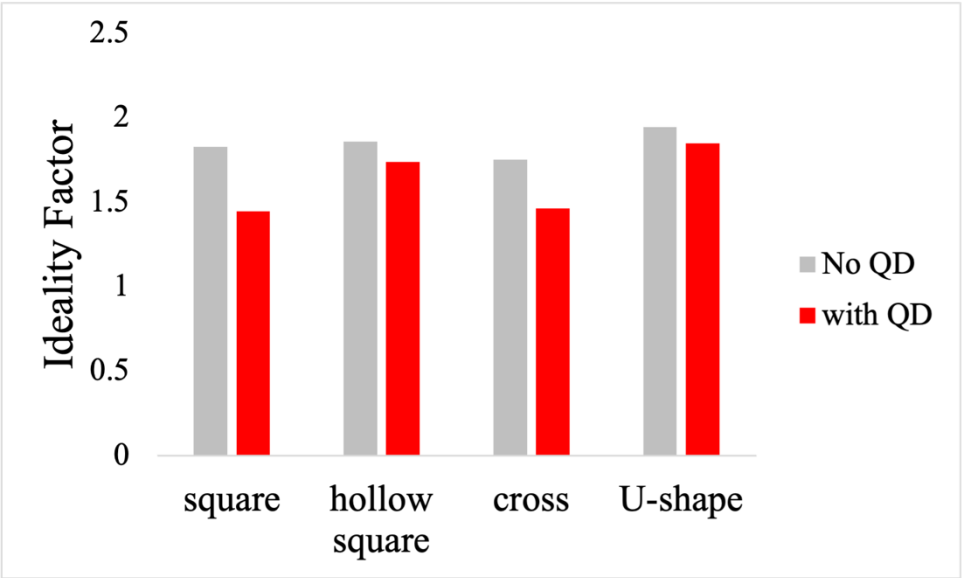

Figure 4.33 PECVD 2000um ideality factor comparison

doi:10.6342/NTU202500081

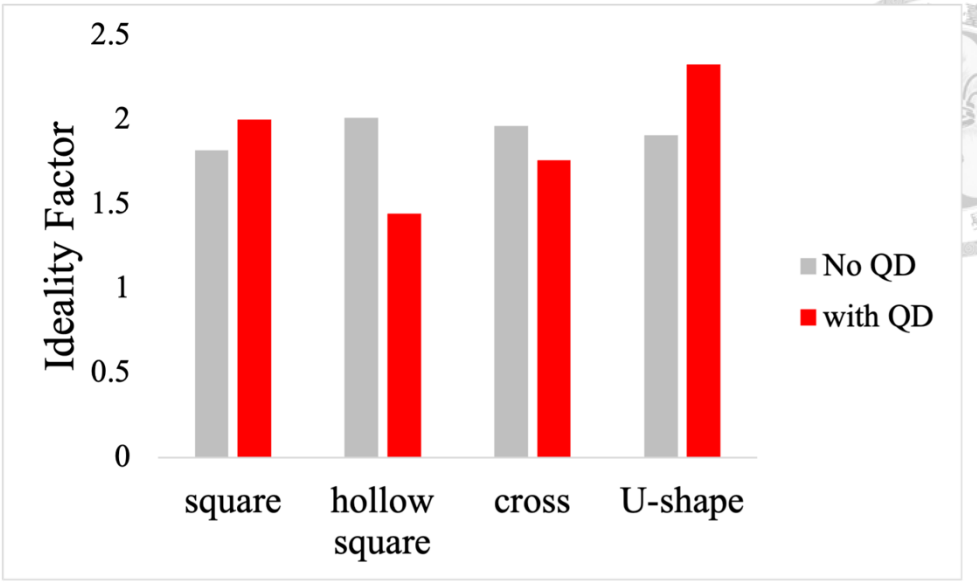

Figure 4.34 ALD 2000um ideality factor comparison

4.3.6 PCE

Although adding QDPR slightly impacts the device's basic performance in terms of fill factor, series resistance, and ideality factor, the PCE of the device still improves due to QD down-conversion.

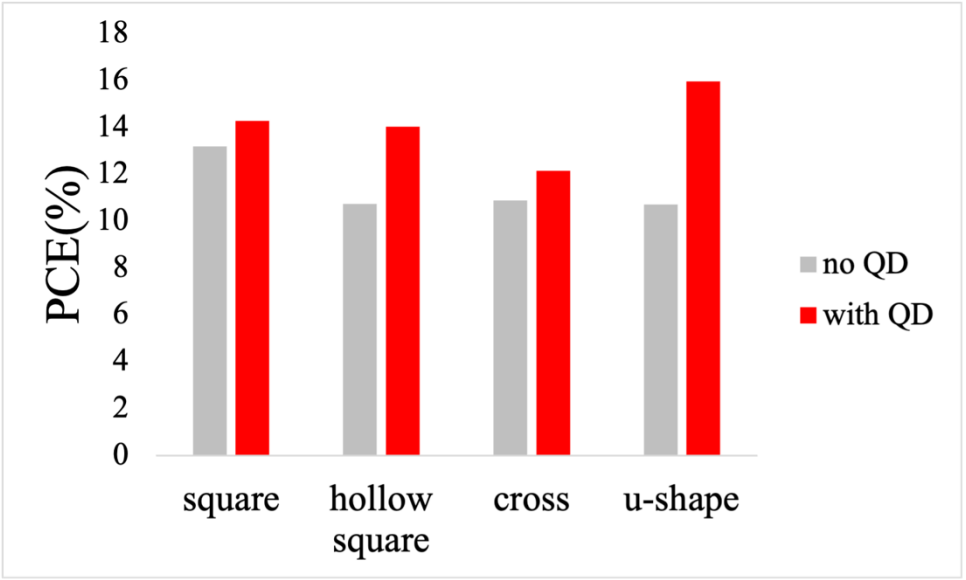

Figure 4.35 PECVD 2000um PCE comparison

doi:10.6342/NTU202500081

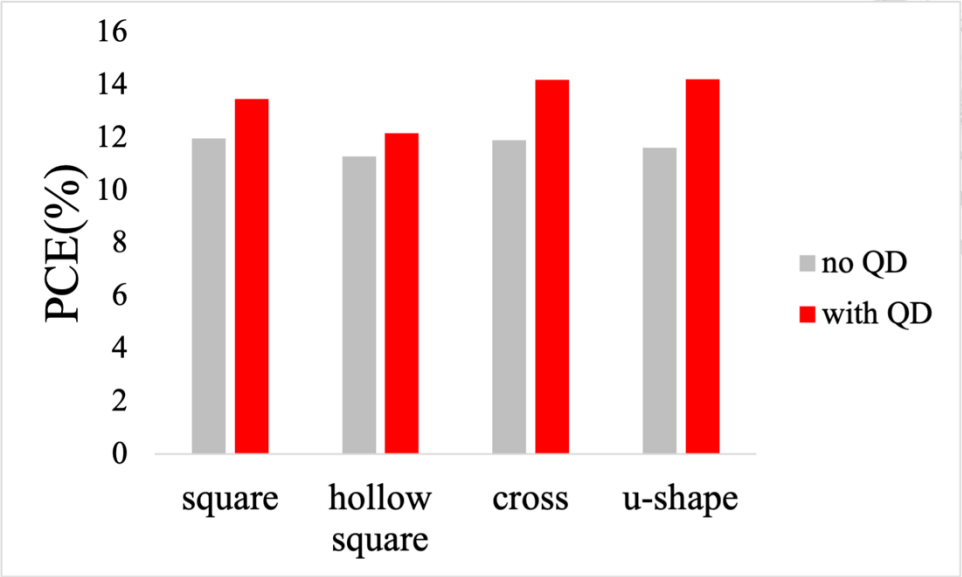

Figure 4.36 ALD 2000um PCE comparison

doi:10.6342/NTU202500081

Chaptor 5 Triple Junction Solar Cell

While working on single-junction devices, we have also been striving to develop triple-junction solar cells. This chapter will discuss the methods we have attempted in this chaptor.

5.1 Material analysis

We purchased epitaxial wafers for triple-junction solar cells from Lichuang Optoelectronics and assumed the structure as shown in Figure 5.1. To verify this assumption, we conducted EDS analysis, with results shown in Figures 5.2 to 5.5, confirming that the wafer's top surface is GaAs. The front-side n-contact consists of Ti/Ag/Au, and the backside p-contact is Ag. Thus, we performed wet etching (30%H2O2:NH4OH=250:1)[27, 28] to remove the surface GaAs layer before depositing metal contacts.

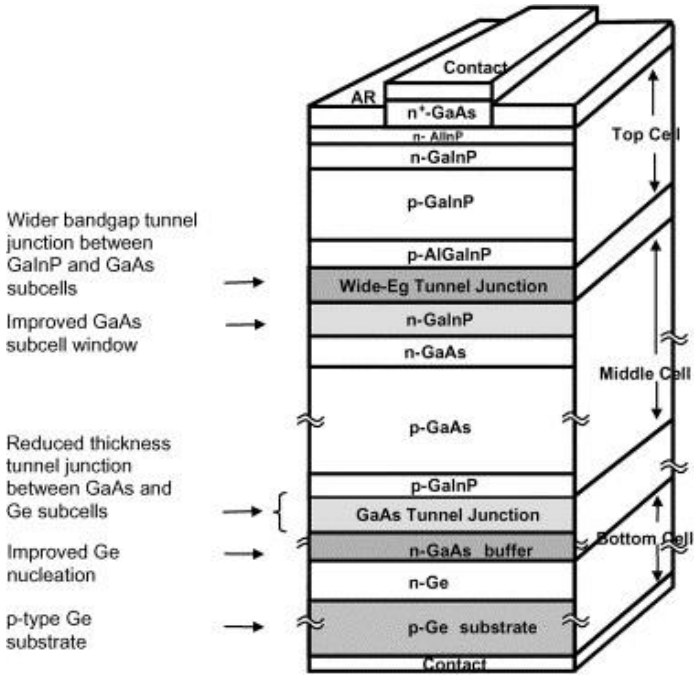

Figure 5.1Diagram of processed triple junction solar cell[29]

doi:10.6342/NTU202500081

Element	At. No.	Line s.	Netto	Mass Norm. [%]	Atom [%]	abs. error [%] (1 sigma)	abs. error [%] (2 sigma)	abs. error [%] (3 sigma)
Phosphorus	15	K-Serie	3017	0.55	1.29	0.05	0.10	0.14
Gallium	31	L-Serie	126036	45.10	46.90	2.41	4.83	7.24
Arsenic	33	L-Serie	147574	52.07	50.38	2.45	4.90	7.36
Indium	49	L-Serie	5726	2.27	1.44	0.10	0.21	0.31
			Sum	**100.00**	**100.00**			

Figure 5.2 EDS of surface of epi wafer

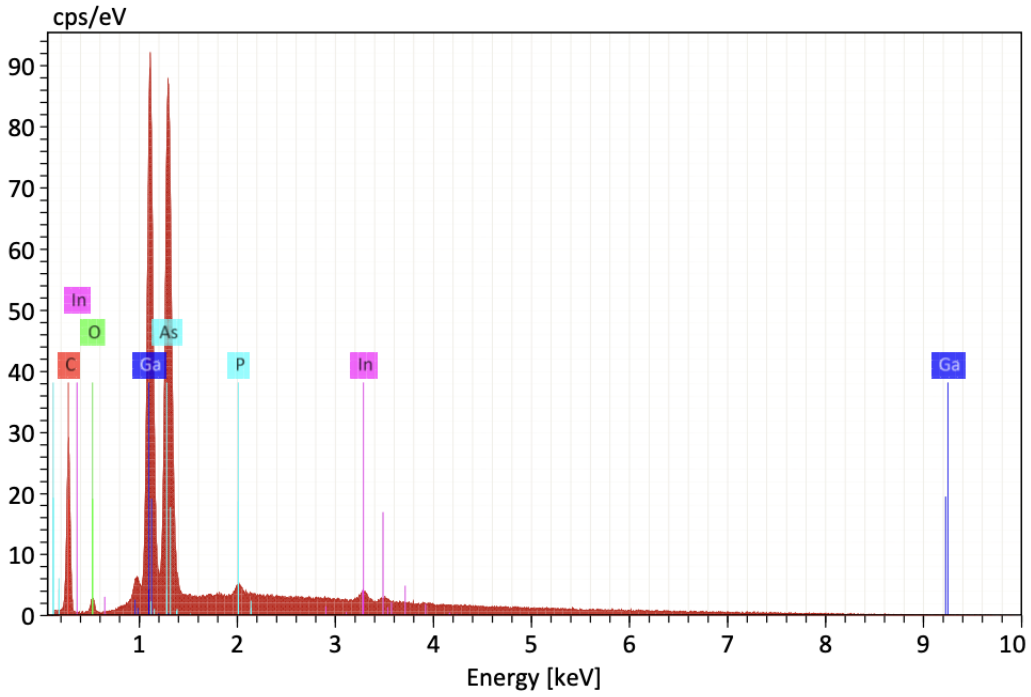

Figure 5.3 EDS of surface of epi wafer

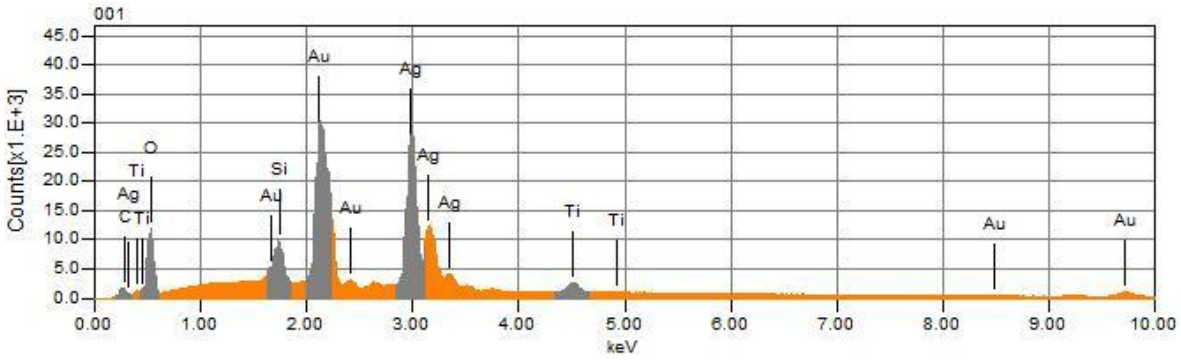

Figure 5.4 Front contact analysis

doi:10.6342/NTU202500081

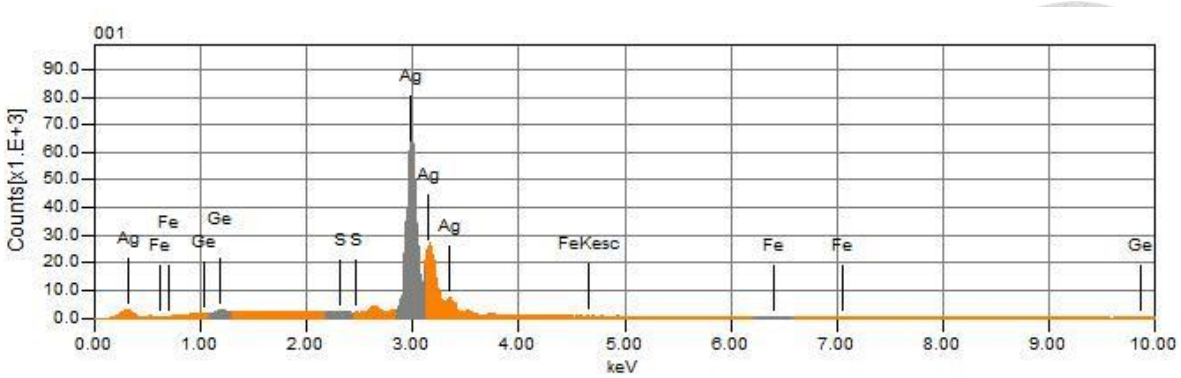

Figure 5.5 Back contact analysis

5.2 Results

The light I-V results did not meet our expectations, and the cause is still under investigation.

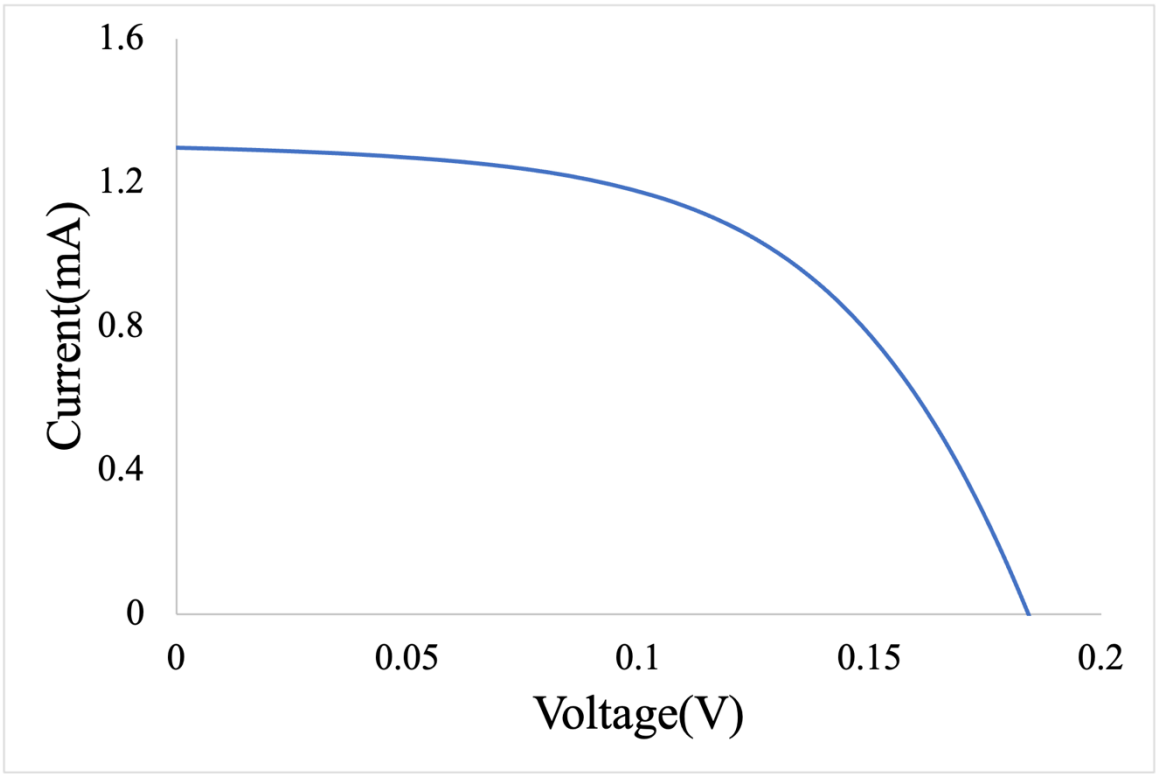

Figure 5.6 Triple junction light IV

doi:10.6342/NTU202500081

Chaptor 6 Conclusion and future work

6.1 Conclusion

We fabricated two types of devices (PECVD/ALD+PECVD) and compared their differences, as well as the changes in characteristics after adding QDPR to the sidewalls. The ALD+PECVD device showed more stability than PECVD. After adding QDPR, both devices showed improvements in PCE, Jsc, and EQE, especially with the Hollow square and Cross shape designs. However, slight declines in fill factor, series resistance, and ideality factor remain areas for future improvement. We are continuing our efforts on triple-junction devices. Although the results are not ideal, we will continue researching until we achieve successful outcomes.

6.2 Future work

Our current results indicate that QDPR has a positive impact on GaAs solar cells, and identifying the optimal QDPR process parameters is our primary goal for improvement. However, due to the limited number of devices fabricated so far, we have not yet observed statistically significant trends, and further investigation is required to determine the optimal design. Based on our dark current measurements, the perimeter-to-area ratio has a certain impact on device performance. Furthermore, the correlation between mesa orientation and perimeter recombination current, as discussed in the literature, will also be included in our

doi:10.6342/NTU202500081

future research.

In addition, the current design does not fully utilize all the light emitted by QDPR. Introducing a Distributed Bragg Reflector (DBR) to enhance directional QD light guidance might maximize light utilization efficiency.[30]

doi:10.6342/NTU202500081

Reference

[1] Ş. Oktik, "The Holy Triangle of Science, Technology and Industry for Photovoltaic Solar Energy Conversion," in *Renewable Energy Based Solutions*, T. S. Uyar and N. Javani Eds. Cham: Springer International Publishing, 2022, pp. 51-80.

[2] G. Raisbeck, "THE SOLAR BATTERY," *Scientific American*, vol. 193, no. 6, pp. 102-111, 1955. [Online]. Available: http://www.jstor.org/stable/24943814.

[3] E. G. Peter, "The Development of Solar Power Satellites," in *Advances in Energy Systems and Technology*, P. Auer Ed.: Academic Press, 1979, pp. 1-48.

[4] D. E. Carlson and C. R. Wronski, "Amorphous silicon solar cell," *Applied Physics Letters*, vol. 28, no. 11, pp. 671-673, 1976, doi: 10.1063/1.88617.

[5] C. Becker *et al.*, "Polycrystalline silicon thin-film solar cells: Status and perspectives," *Solar Energy Materials and Solar Cells*, vol. 119, pp. 112-123, 2013.

[6] R. C. Knechtli, R. Y. Loo, and G. S. Kamath, "High-efficiency GaAs solar cells," *IEEE Transactions on electron devices*, vol. 31, no. 5, pp. 577-588, 1984.

[7] M. Yamaguchi, T. Takamoto, K. Araki, and N. Ekins-Daukes, "Multi-junction III–V solar cells: current status and future potential," *Solar Energy*, vol. 79, no. 1, pp. 78-85, 2005.

[8] K.-L. Liang *et al.*, "Highly Efficient Fine-Pitch Quantum Dot/Titanium Oxide Nanocomposites for Ultrahigh-Resolution Full-Color Micro-Light Emitting Diode Displays," *ACS Photonics*, vol. 11, no. 8, pp. 2981-2991, 2024.

[9] E. Klampaftis, D. Ross, K. R. McIntosh, and B. S. Richards, "Enhancing the performance of solar cells via luminescent down-shifting of the incident spectrum: A review," *Solar energy materials and solar cells*, vol. 93, no. 8, pp. 1182-1194, 2009.

[10] H.-C. Chen *et al.*, "Enhancement of power conversion efficiency in GaAs solar cells with dual-layer quantum dots using flexible PDMS film," *Solar Energy Materials and Solar Cells*, vol. 104, pp. 92-96, 2012/09/01/ 2012, doi: https://doi.org/10.1016/j.solmat.2012.05.003.

[11] S.-C. Hsu, Y.-M. Huang, Y.-C. Kao, H.-C. Kuo, R.-H. Horng, and C.-C. Lin, "The analysis of dual-junction tandem solar cells enhanced by surface dispensed quantum dots," *IEEE Photonics Journal*, vol. 10, no. 5, pp. 1-11, 2018.

[12] P. Würfel and U. Würfel, *Physics of solar cells: from basic principles to advanced concepts*. John Wiley & Sons, 2016.

[13] J. Nelson, "The physics of solar cells," *Imperial College Press google schola*, vol. 2, pp. 62-68, 2003.

doi:10.6342/NTU202500081

[14] F. A. Lindholm, J. G. Fossum, and E. L. Burgess, "Application of the superposition principle to solar-cell analysis," *IEEE transactions on electron devices*, vol. 26, no. 3, pp. 165-171, 1979.

[15] G. Araujo and E. Sanchez, "Analytical expressions for the determination of the maximum power point and the fill factor of a solar cell," *Solar Cells*, vol. 5, no. 4, pp. 377-386, 1982.

[16] H. Bayhan and M. Bayhan, "A simple approach to determine the solar cell diode ideality factor under illumination," *Solar Energy*, vol. 85, no. 5, pp. 769-775, 2011.

[17] R. Handy, "Theoretical analysis of the series resistance of a solar cell," *Solid-State Electronics*, vol. 10, no. 8, pp. 765-775, 1967.

[18] T. Gu, M. A. El-Emawy, K. Yang, A. Stintz, and L. F. Lester, "Resistance to edge recombination in GaAs-based dots-in-a-well solar cells," *Applied Physics Letters*, vol. 95, no. 26, 2009.

[19] Y.-Y. Cho *et al.*, "The Luminescent Down Shifting Effect of Single-Junction GaAs Solar Cell with Perovskite Quantum Dots," in *2019 IEEE 46th Photovoltaic Specialists Conference (PVSC)*, 2019: IEEE, pp. 2600-2602.

[20] M. Tong, K. Nummila, A. Ketterson, I. Adesida, L. Aina, and M. Mattingly, "Selective wet etching characteristics of lattice-matched InGaAs/InAlAs/InP," *Journal of The Electrochemical Society*, vol. 139, no. 10, p. L91, 1992.

[21] S. Sioncke *et al.*, "Etch rates of Ge, GaAs and InGaAs in acids, bases and peroxide based mixtures," *ECS Transactions*, vol. 16, no. 10, p. 451, 2008.

[22] W. Lim *et al.*, "Investigation of GaAs dry etching in a planar inductively coupled BCl3 plasma," *Journal of the Electrochemical Society*, vol. 151, no. 3, p. G163, 2004.

[23] P. Vigneron, F. Joint, N. Isac, R. Colombelli, and E. Herth, "Advanced and reliable GaAs/AlGaAs ICP-DRIE etching for optoelectronic, microelectronic and microsystem applications," *Microelectronic Engineering*, vol. 202, pp. 42-50, 2018.

[24] A. Belghachi and S. Khelifi, "Modelling of the perimeter recombination effect in GaAs-based micro-solar cell," *Solar energy materials and solar cells*, vol. 90, no. 1, pp. 1-14, 2006.

[25] C. Pellegrino, A. Gagliardi, and C. G. Zimmermann, "Impact of proton and electron irradiation-induced defects on the dark current of GaAs solar cells," *IEEE Journal of Photovoltaics*, vol. 9, no. 6, pp. 1661-1667, 2019.

[26] Y. Zhang, G. Wu, F. Liu, C. Ding, Z. Zou, and Q. Shen, "Photoexcited carrier dynamics in colloidal quantum dot solar cells: insights into individual quantum dots, quantum dot solid films and devices," *Chemical Society Reviews*, vol. 49, no. 1, pp. 49-84, 2020.

[27] W. P. Gomes, "Wet etching of III–V semiconductors," in *Handbook of Advanced Electronic and Photonic Materials and Devices*: Elsevier, 2001, pp. 221-256.

doi:10.6342/NTU202500081

[28] A. Clawson, "Guide to references on III–V semiconductor chemical etching," *Materials Science and Engineering: R: Reports,* vol. 31, no. 1-6, pp. 1-438, 2001.

[29] N. H. Karam *et al.*, "Recent developments in high-efficiency Ga0. 5In0. 5P/GaAs/Ge dual-and triple-junction solar cells: steps to next-generation PV cells," *Solar Energy Materials and Solar Cells,* vol. 66, no. 1-4, pp. 453-466, 2001.

[30] T. Stellwag, M. R. Melloch, M. S. Lundstrom, M. Carpenter, and R. Pierret, "Orientation-dependent perimeter recombination in GaAs diodes," *Applied physics letters,* 1990.

doi:10.6342/NTU202500081